Journal of Building Engineering 84 (2024) 108568

Contents lists available at ScienceDirect

Journal of Building Engineering

journal homepage: www.elsevier.com/locate/jobe

# Investigation of waste clay brick (chamotte) addition and activator modulus in the properties of alkaline activation cements based on construction and demolition waste

A. García-Díaz [a], P. Delgado-Plana [a,b], S. Bueno-Rodríguez [a,b], D. Eliche-Quesada [a,b,*]

[a] Department of Chemical, Environmental and Materials Engineering, Higher Polytechnic School of Jaén, University of Jaén, Campus Las Lagunillas, 23071, Jaén, Spain

[b] Center for Advanced Studies in Earth Sciences, Energy and Environment (CEACTEMA), University of Jaén, Campus Las Lagunillas s/n, 23071, Jaén, Spain

ARTICLE INFO

*Keywords:*
Construction and demolition wastes
Chamotte
Alkaline activated cements
Activator modulus
Mechanical properties

ABSTRACT

The use of construction and demolition waste (CDW) as a raw material for the manufacture of alkali-activated cements (AACs) is a promising and sustainable way to recover construction waste. CDW mainly consists of mineral residues such as concrete and ceramic waste. In this study, CDW with a high fraction of concrete waste is used, so the enrichment effect of the waste in the ceramic fraction is studied. For this purpose, different proportions of chamotte (CHM) have been incorporated (0–40 wt%). The CDW precursor or CDW-CHM precursors have been activated using 8 M sodium hydroxide and sodium silicate solution, using an activator modulus (mol $SiO_2$/mol $Na_2O$ = Ms = 1.0) and the specimens were cured at room temperature. The liquid/binder ratio was 0.45 for all the pastes manufactured. The results indicate that the progressive enrichment of the ceramic fraction or the incorporation of CHM results in alkaline activated cements (AACs) with similar physical properties such as bulk density, water absorption and total porosity, but with improved mechanical properties. The incorporation of 40 wt% CHM results in optimum compressive strengths with values of 29.7 and 41.2 MPa after 28 and 56 days of curing respectively, higher than those obtained for the control specimens containing only CDW 15.2 MPa and 30.65 MPa respectively. Subsequently, the impact of the silicate modulus of the alkaline activator (Ms = 0.5; 1.0 and 2.0) on the performance of the AACs was evaluated in the control cement and in the optimum cement incorporating 40 wt% CHM. The mechanical performance of the AACs improves substantially with increasing activator modulus up to a certain threshold Ms = 1.0, but finally decreases slightly with Ms = 2.0. Therefore, this study demonstrates the possibility of valorising wastes from the construction sector through their use as precursors in the manufacture of environmentally friendly alkaline activated cements with macroscopic performances that improve with the content of the ceramic fraction (CHM).

## 1. Introduction

Construction as it is conceived is one of the least sustainable activities on the planet [1]. In fact, this sector is responsible for 25–35

* Corresponding author. Department of Chemical, Environmental and Materials Engineering, Higher Polytechnic School of Jaén, University of Jaén, Campus Las Lagunillas, 23071, Jaén, Spain.
*E-mail address:* deliche@ujaen.es (D. Eliche-Quesada).

https://doi.org/10.1016/j.jobe.2024.108568
Received 2 August 2023; Received in revised form 19 December 2023; Accepted 14 January 2024
Available online 18 January 2024

% of total waste generation, 5–12 % of total greenhouse gas emissions and 42 % of the European Union's energy consumption [2–4]. Among these consequences, high volumes of construction and demolition waste (CDW) have become a major environmental problem, representing up to 30 % of the solid waste generated worldwide [5,6]. The origin of CDW is diverse: waste generated during the construction of new buildings, waste originating from the renovation and demolition of infrastructure, waste from natural disasters or military conflicts [5]. This type of waste is very heterogeneous and may contain: concrete, mortar, bricks, plaster, tiles, sanitary ceramics, wood, glass, aggregates, asphalt, bituminous mixtures, tar, metallic materials and plastics among others [4–10]. It is estimated that approximately 87 % of this waste consists mainly of mineral debris such as concrete and ceramic debris [11]. Due to its alarming generation, amounting to 850 million tonnes per year in Europe [8,12,13], and exceeding 3 billion tonnes per year worldwide [2], the management of this type of waste has become both a social and environmental problem. Since, unfortunately, almost 43 % of the CDW generated in Europe ends up in landfills, posing significant environmental, economic, social and public health problems due to its characterisation as non-biodegradable [13]. Therefore, the recycling of CDW is of paramount importance since, being heavy and bulky waste, it is not desirable for landfill disposal, and its recycling is environmentally significant as it would reduce the consumption of energy and natural resources, as well as $CO_2$ emissions [8].

To date, the main use of CDW is as a partial replacement of natural aggregates to produce mortars and concretes, and it is also used in geotechnical applications, such as slope stabilisation, foundations, granular bases and subgrade bases [2,6,14]. It is also used in civil applications as a construction material for unpaved, low-traffic roads, embankments and trench backfill, and can also be used in bituminous mixtures [4,15]. However, the above uses do not represent a solution to the global CDW problem. Therefore, the search for recycling alternatives that ensure the real use of CDW is a priority worldwide [2]. One of the most interesting solutions for the utilization of this type of waste is its use as a precursor in alkaline activation technology or "geopolymerisation" [2,16]. Such technology is considered an ideal option to recycle RCD's flows as new value-added products [13] due to the RCD's mainly composed of silicon materials [5], more or less enriched in calcium, which, in alkaline medium, suffer a series of chemical reactions that give place to alkali gels from aluminosilicatos characterized by a partial or fully amorphous polymeric structure that consists of Si-O-Al links with cementing properties [17,18]. For this reason, geopolymers or alkali-activated cements are alternative binders to Portland cement [16]. This option has advantages from both an environmental and technological point of view, since its synthesis is carried out at a relatively low temperature (below 100 °C), as it does not require sintering, which allows for a significant reduction in both greenhouse gas emissions and energy consumption. In addition, it reduces the consumption of natural raw materials as it reuses solid waste to obtain materials that can provide performance comparable to OPC or even with higher mechanical strength and lower porosity, which is beneficial for many industrial applications [19,20]. Among the wide variety of properties and characteristics of these new binders are high compressive strength, low shrinkage, fast or slow setting, acid resistance, fire resistance, resistance to freeze-thaw cycling and low thermal conductivity [3], all of which depend mainly on the mineralogy of the raw materials as well as the alkaline activator used [18]. The main difficulty of using CDW on a large scale is related to its high heterogeneity and, consequently, its low reproducibility. Therefore, most studies have focused on using specific parts of this waste [1,6]. Moreover, as can be seen in the studies carried out by other authors on this residue, in most cases, curing heat treatments between 50 and 90 °C are applied to achieve adequate mechanical strengths [2]. Ahmari et al. [18] produced a geopolymer binder from mixtures of waste concrete and fly ash using 10 M NaOH solutions as activator, the compressive strength of the final products reached almost 30 MPa. Komnitsas et al. [7] studied the synthesis of geopolymers from three fractions of CDR: concrete, ceramic bricks and ceramic tiles. The curing time was 7 days at three temperatures 60, 80 or 90 °C. The tile-based mixtures reached a maximum of 58 MPa, while the brick-based and concrete-based mixtures showed lower strength values of 35 MPa and 13 MPa, respectively. However, it should be noted that such compressive strength values were only possible using high curing temperatures of 80 or 90 °C. Vásquez et al. [7] activated CDW used an activator composed of sodium hydroxide and sodium silicate, cured at room temperature for 28 days. They obtained compressive strengths in the order of 25 MPa with a 100 % CDW geopolymer, 33 MPa with a hybrid geopolymer (70 % CDW + 30 % Portland cement) and 46 MPa with a binary geopolymer (90 % CDW + 10 % metakaolin).

On the other hand, waste bricks constitute an important fraction of CDW [21]. Conventional bricks are produced from a mixture of clays with added sand and then fired in a kiln at a temperature between 850 and 950 °C [22]. Their annual worldwide production is approximately 1400 billion units and demand are expected to increase steadily [3,5]. However, this industry is also related to numerous environmental problems, because the production process of clay bricks consumes large amounts of energy, especially in the sintering stage. Furthermore, it requires the extraction of natural raw materials such as clay, sand, silt, etc. and releases huge amounts of greenhouse gases into the atmosphere [19,23]. Apart from the environmental problems, there is also the generation of a large volume of solid waste, as the ceramic waste generated after the sintering step cannot be re-incorporated into the production process and those that do not have the right characteristics are disposed of in inappropriate places causing damage to the environment [17]. These wastes are generated by failures in the sintering stage that form products with inappropriate visual appearance, presenting some physical defect, technological problems, deviations of geometrical values that do not meet market requirements or breakages in transport [19,24,25]. So far, a large part is used in landfills [26], however, this practice causes many environmental problems [27] due to impacts related to soil and water contamination, air pollution as a result of possible fires, destruction of landscape and open spaces, and reduction of land value [9]. In order to reduce their volume, a common practice is to crush the bricks and then deposit them in the vicinity of industries with the consequent environmental impact, this crushed material is called chamotte [25]. This chamotte is often recycled as a filler and stabilisation material for infrastructure, as a sub-base for roads in landscaping, as coarse aggregate for concrete production, as sand for paving tennis courts, etc. [28,29]. However, its properties are not optimised in these processes [25]. As in the case of CDW, the amount of chamotte that is reused is still negligible [26]. Therefore, its reuse in other industries is a necessary task. Since, most of the composition of chamotte is silica and alumina with a large number of amorphous phases, presenting pozzolanic activity [17,27,29,30] these wastes have the potential to be used as precursors for alkaline activated materials [17,25,27,29,30].

Moreover, in contrast to CDW, since the production process of ceramic bricks is similar between different companies, as well as the raw material used, there is a repeatability of the properties of the by-product over time [25]. Consequently, recycling and reusing both CDW and chamotte as precursors for alkali-activated cements can offer a sustainable solution to reduce the ecological impact and decrease the demand for OPCs [19].

On the other hand, the alkaline activator plays a crucial role in the geopolymerisation process. The most commonly used alkaline activators are MOH-type caustic alkalis (M = Na or K) and $R_2O(n)SiO_2$-type silicates, mainly sodium silicate ($Na_2SiO_3$), which are used individually or in combination [31,32]. NaOH provides the hydroxide anion (OH), which is very important for the dissolution of aluminosilicates in the first stage and the subsequent geopolymerisation process, as it acts as a catalyst for the reaction during the activation process. It also provides the sodium alkali metal cation ($Na^+$), which is important for the charge balance of the aluminosilicate network formed in the last stage [20,33–35]. The sodium aluminosilicate (N-A-S-H) gel structure contains Si and Al tetrahedra randomly distributed along the polymer chains that are cross-linked to provide cavities of sufficient size to accommodate the charge-balancing hydrated sodium ions [36]. Although the NaOH solution is important for dissolving the $Si^{4+}$ and $Al^{3+}$ ions from the precursors and thus for the geopolymerisation process. The process at room temperature is very slow, which results in a low strength [35]. Therefore, NaOH is often combined with sodium silicate ($Na_2SiO_3$) [37]. $Na_2SiO_3$ is the chemical component that has a decisive influence on the development and improvement of the strength of alkali-activated cements [31]. It is known that the addition of soluble silica species increases the reactivity rate and promotes the formation of longer silicate oligomer chains which is used to promote the condensation process of alkaline activated cements, thus improving their mechanical properties [32,35]. Therefore, a higher percentage of $Na_2SiO_3$ increases the presence of soluble Si in the activator, favours gel formation, increases the Si/Al ratio, increases the degree of condensation and also increases the mechanical strength [20,32,36,38]. For these reasons, several researchers have reported that the best mechanical performance of the active cemeteries are obtained with combinations of NaOH and $Na_2SiO_3$ solutions [35]. The use of NaOH can be useful to disrupt the Al and Si ions in the precursors, while the inclusion of $Na_2SiO_3$ promotes the process of condensation. However, both solutions have parameters that need to be properly adjusted to be beneficial and improve the properties of the alkaline activated binders. Although $Na_2SiO_3$ increases the content of additional silicate species in the system and thus enhances the geopolymerisation reaction, very high concentrations of soluble silica tend to retard the reactions due to lower pH and increased viscosity of the mixture [32]. Therefore, one of the most important factors affecting the properties of alkaline activated cements is the ratio of NaOH to $Na_2SiO_3$, or activator modulus (mol $SiO_2$/mol $Na_2O$ = Ms).

In view of this background, the novelty of this work lies in the use of CDW with a high fraction of concrete produced in a treatment plant without any previous separation into its fractions, studying the effect of the incorporation of chamotte on the technological properties of AACs cured at room temperature. The synergistic effect of chamotte incorporation to CDW residue not separated in fractions has not been previously studied. Therefore, the main objective of this study is to investigate the feasibility of using CDW with a high fraction of concrete as a precursor in the manufacture of alkaline activated cements. The effect on the macroscopic and microstructural properties of the enrichment of CDW by ceramic fractions through the incorporation of 10-40 wt% of chamotte (CHM) has been studied. In addition, the activator modulus (mol $SiO_2$/mol $Na_2O$) of the control and optimum mix cements has been used as a key parameter to explore the effects on the aforementioned properties. The research results can provide valuable information for the preparation of sustainable alkali activated materials from CDW in the future.

## 2. Materials and methods

### 2.1. Raw materials and characterization

The materials used as precursors are entirely industrial waste from the construction sector.On the one hand, the construction and demolition waste (CDW) has been provided by “Association of Management Companies Construction and Demolition Waste (AGRECA)" of Andalusia located in Cordoba (Spain), on the other hand, the chamotte (CHM) has been obtained from pieces of fired ceramic bricks commercially unsuitable for the market because they are defective pieces supplied by the company Ladrillos Bailén S.A., located in Bailén (Jaén, Spain).

For their use, both materials had to be crushed, first in a hammer mill to reduce the size of the material fragments arriving at the laboratory, and then in a ball mill for 1 h at 350 rpm. Finally, the ground material is sieved below 100 μm. As can be seen in Fig. 1, the CDW particles have a more heterogeneous distribution and a slightly higher average particle size $D_{50}$ = 10.3 μm than the CHM particles

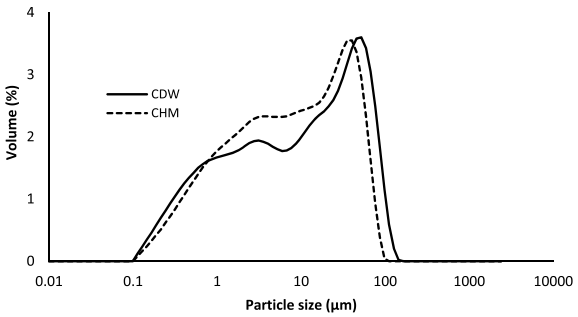


**Fig. 1.** Particle size distribution of raw materials: Construction and demolition waste (CDW) and Chamotte (CHM).

with a particle size $D_{50} = 8.00$ μm and a more homogeneous particle size distribution. On the other hand, both the specific surface area and the real density, obtained through a helium pycnometer, are higher for chamotte than for CDW, being 3068 $m^2$/kg and 2721 kg/$m^3$ for CDW and 3406 $m^2$/kg and 2841 kg/$m^3$ for CHM.

The crystalline mineralogical phases of the raw materials were identified by X-ray diffraction (XRD) with the Empyrean equipment with a PIXcel-3D detector from PANalytical using Cu K-α radiation (λ = 1.5406 Å) at a voltage of 40 kV and an amperage of 40 mA, a 2-theta range of 10 to 60° and a step size of 0.02. For phase identification, the HighScore software was used.

The CDW diffraction pattern (Fig. 2a) shows a semi-crystalline nature with the main crystalline phase being $SiO_2$ (Ref cod. 96-500-0036). Other phases were also identified, such as soda-calcium feldspars belonging to the plagioclase group (albite and anorthite) (Ref cod. 96-155-7000 and 96-100-0035), phyllosilicates such as illite (Ref cod. 96-901-3719), calcite ($CaCO_3$) (Ref cod: 96-901-6707) and dolomite (Ref cod: 96-900-4931). Whereas, for the CHM residues (Fig. 2b), $SiO_2$, quartz (Ref. cod. 96-901-2601), hematite, $Fe_2O_3$ (Ref. cod. 96-900-0140), illite (Ref. cod. 96-900-9666), plagioclase as albite (Ref. cod. 96-155-6999) and alkali feldspars (Ref. cod. 96-591-0069) are identified as crystalline phases. The information of phases are shown in Table 1.

The identification of functional groups was carried out by attenuated total reflectance Fourier transform infrared spectroscopy (ATR-FTIR) using the Vertex 70 Bruker in the range 4000-400 $cm^{-1}$.

In the CDW (Fig. 3a) and CHM, the bands centered at 1400, 860 and 700 $cm^{-1}$ suggesting the presence of O-C-O bonds of $CO_3^{2-}$ groups associated with carbonate phases originated by the presence of calcite in the original precursor, indicating a higher amount of calcium oxide in the residue CDW [7]. The main band centered at 994 $cm^{-1}$ en CDW and a 969 $cm^{-1}$ en el precursor CHM, corresponding to the assimetric stretching vibrations of the Si-O-Si and Si-O-Al bonds of typical of aluminosilicate species [1,7]. The peak centered at the 453 $cm^{-1}$ frequency en CDW y 441 $cm^{-1}$ en CHM is assigned to Si-O and Al-O bending vibrations in the tetrahedral structure of precursors [7,27]. The doublet at 782–763 $cm^{-1}$ as well as the peak at around 542 $cm^{-1}$ are attributed to Si–O–Si inter tetrahedral bridging bonds in $SiO_2$ which indicates the presence of quartz mineral [22]. The bands of about 450–780 $cm^{-1}$ detected in all specimens would be associated with the bending of Si–O in the plane and Al–O bonds, as well as bending vibrations Si–O–Si and O–Si–O [1].

The chemical composition of the raw materials was determined by X-ray fluorescence (XRF) using a Philips Magix Pro model PW-2440 instrument and the results are given in Table 2. In the case of CDW, $SiO_2$ (51.7 wt%) and CaO (18.9 wt%) predominate, whereas, $Al_2O_3$ is limited to 5.9 wt %. Furthermore, the loss on ignition (LOI) of the CDW precursor is 15.5 wt%. The CHM residue has mainly a high $SiO_2$ content (63.1 wt%), with significant additional contents of $Al_2O_3$ (12.1 wt %), CaO (8.7 wt%) as well as $Fe_2O_3$ (4.7 wt%). These data confirm the XRD patterns of both materials, where quartz-phase silica predominates.

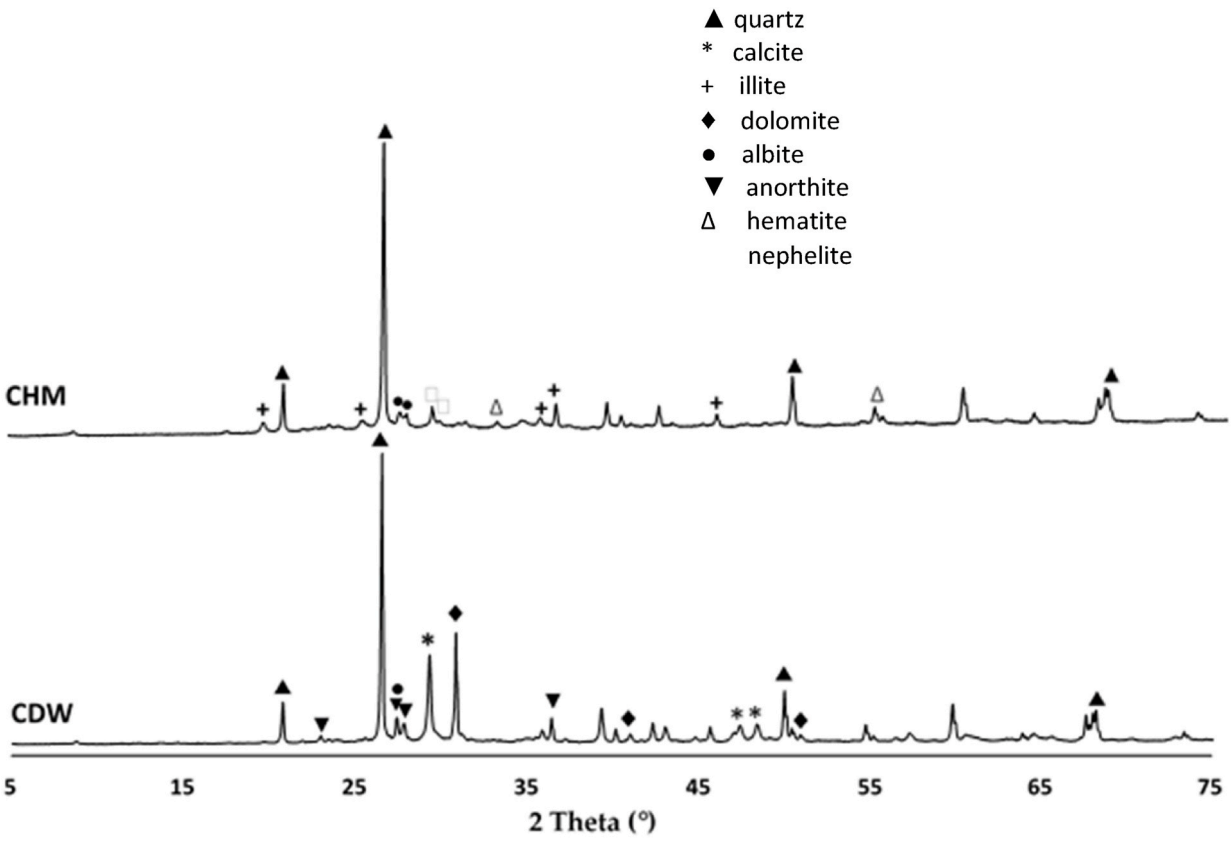


**Fig. 2.** XRD patterns of raw materials: (a) Construction and demolition waste (CDW) and b) Chamotte (CHM).

**Table 1**
Crystalline phases information.

| Symbol | Phase | PDF card No. | 2θ (°) |
|---|---|---|---|
| ▲ | quartz | 96-901-2601 | 20.857, 26.637, 50.146, 68.063 |
| * | calcite | 96-901-6707 | 29.437, 47.467, 48.568 |
| + | illite | 96-901-3719 | 20.431, 24.364, 35.191, 45.213 |
| ◆ | dolomite | 96-900-4931 | 30.917, 41.092, 50.725 |
| ● | albite | 96-155-7000 | 27.785 |
| ▼ | anorthite | 96-100-0035 | 22.002, 27.347, 27.938, 35.915 |
| Δ | hematite | 96-900-0140 | 33.118, 54.004, |
| | nephelite | 96-591-0069 | 29.263, 30.670 |

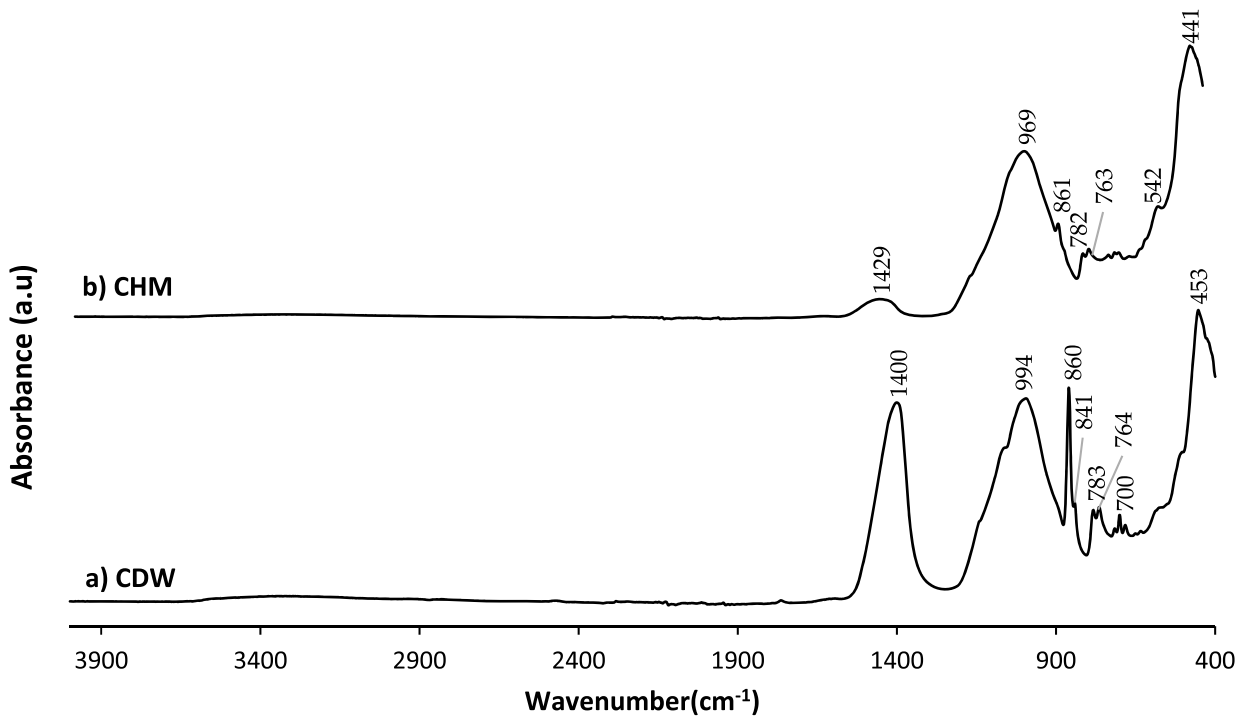


**Fig. 3.** FTIR patterns of raw materials: (a) Construction and demolition waste (CDW) and b) Chamotte (CHM).

**Table 2**
Chemical composition of raw materials (wt %): Construction and demolition waste (CDW) and Chamotte (CHM).

| | $SiO_2$ | $Al_2O_3$ | $Fe_2O_3$ | CaO | MgO | $Na_2O$ | $K_2O$ | LOI |
|---|---|---|---|---|---|---|---|---|
| **Construction and demolition waste (CDW)** | 51.69 | 5.93 | 2.46 | 18.93 | 2.05 | 0.63 | 1.43 | 15.54 |
| **Chamotte (CHM)** | 63.08 | 12.11 | 4.67 | 8.67 | 1.88 | 0.47 | 3.25 | 3.60 |

The morphology of the raw materials (Fig. 4) were obtained using Scanning Electron Microscopy (SEM) using a JEAL model SM 840 assisted by Energy Dispersive X-ray Spectroscopy (EDS). The samples were placed on an aluminium grid and carbon coated using the JEOL JFC 1100 sputter coater.

In the CDW residue (Fig. 4a), spherical, slightly rounded and irregular particles can be observed, while in the CHM residue, there are no spherical particles. Although, in both precursors, particles of different sizes can be observed, smaller particle sizes are observed in the CHM residues according to the particle size distribution data obtained (Fig. 1). Furthermore, the microanalysis performed on the selected samples shown in Fig. 4 reveals the presence of irregular particles rich in silicon, calcium and, to a lesser extent, aluminium (Spectrum 1) in the CDW and richer in silica and alumina and lower in calcium in the chamotte residue (Spectrum 4). The slightly rounded particles are richer in calcium and are observed in both residues (Spectrum 2). While the spherical particles present only in the CDW residue are rich in silica (Spectrum 3).

### *2.2. Alkali-activated cement preparation and characterization*

To make up the various test samples, the activating solution is first prepared and then the precursors are mixed. In a first series, the

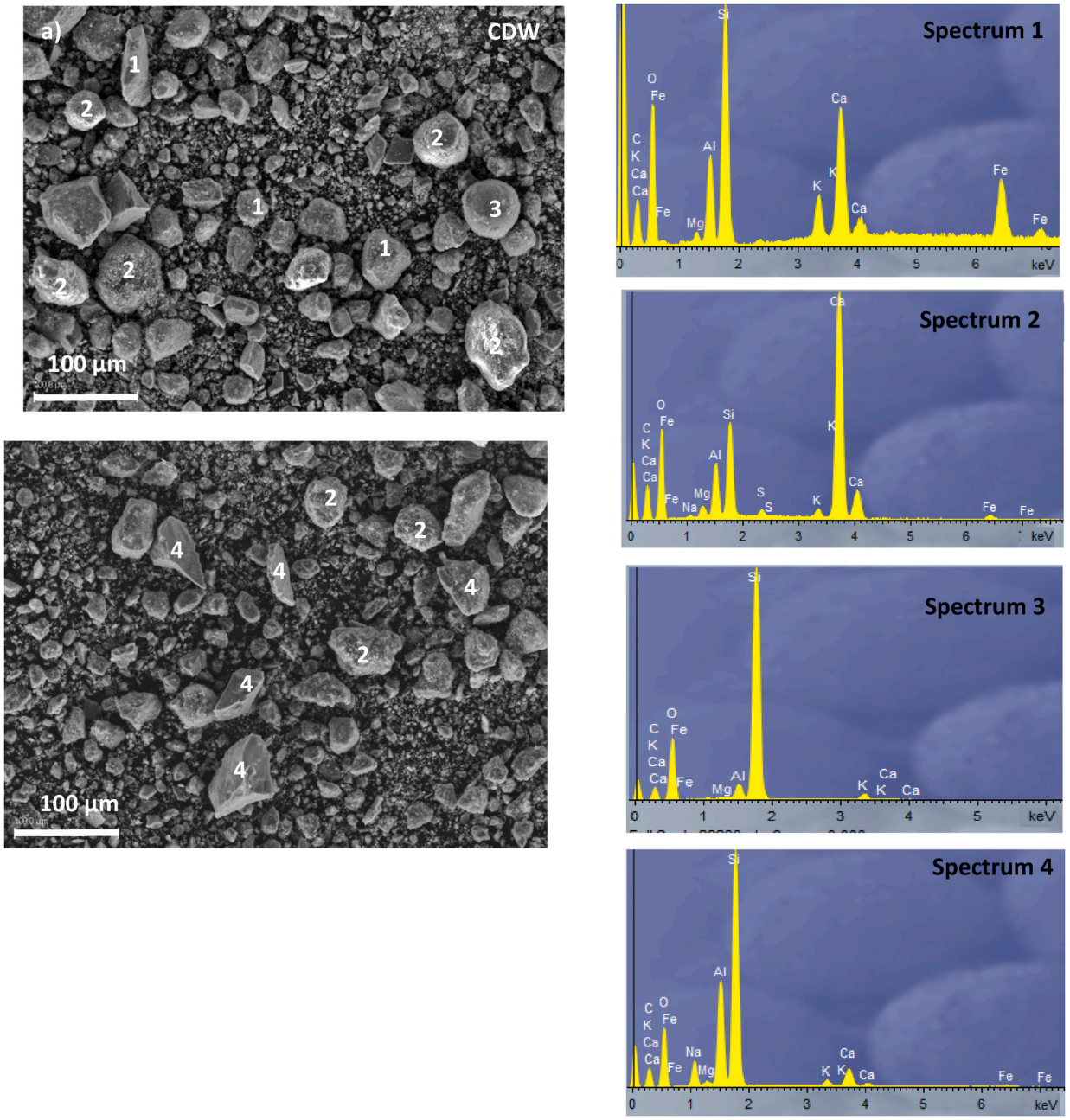


**Fig. 4.** SEM micrographs and EDS analysis of raw materials: a) Construction and demolition waste (CDW) and b) Chamotte (CHM).

CDW (standard mixture) is taken as a base, and increasing percentages of CHM are added from 10 wt% to 40 wt%, with increments of 10 wt%, always using the same alkaline activator with an activator modulus = Ms = mol $SiO_2$/mol $Na_2O$ = 1.0). The influence of the incorporation of different amounts of CHM on the physical and mechanical properties of alkaline activated cements has been studied. Once the CDW-CHM precursor mixture was optimised, a second series of mixtures was carried out, in which the influence of the activator modulus (Ms = 0.5; 1.0 and 2.0) was studied in both the control sample and the optimum 60CDW-40CHM.

### 2.2.1. *Alkaline solution*

A commercial alkaline solution with sodium hydroxide (NaOH) (98 % purity, Panreac) and sodium silicate ($Na_2SiO_3$) (29.2 % $SiO_2$; 8.9 % $Na_2O$; and 61.9 % $H_2O$, Panreac) was used as alkaline activator. For its preparation, the required NaOH granules are first weighed and, with the help of a magnetic stirrer, dissolved in distilled water to obtain an 8 M concentration (Table 3). Once the aqueous solution has cooled, the required amount of sodium silicate ($Na_2SiO_3$) is added in liquid form to obtain the desired activator modulus and homogenised again using a magnetic stirrer (Table 3). For example, to obtain an activator modulus Ms = 0.5, 33.23 g of

NaOH are dissolved in 101.77 g of distilled $H_2O$, to obtain an 8 M solution, once it is cold, 45.00 g $Na_2SiO_3$ are added.

Taking into account the heat generated during preparation, the alkaline solutions are allowed to cool at room temperature for 24 h before use. Finally, the pH is measured with a Crison Basic 20 pH meter. The alkaline activator is one of the most important factors affecting the development of the matrix strength of alkaline activated cements. The NaOH solution is important for dissolving the $Si^{4+}$ and $Al^{3+}$ ions of the precursors, while the $Na_2SiO_3$ solution is used to promote the condensation process of the geopolymerisation process, acting as a binder [10,19].

### 2.2.2. Preparation of alkaline activation cements

The mixtures of alkali-activated cements were prepared in a Proeti planetary mixer using the same sequence for all compositions. First, the dry raw materials, CDW and CHM, were mixed and homogenised for 90 s at low speed (140 ± 5 rpm). After this time, the activator solution was added to the homogeneous mixture and mixed at low speed for another 90 s. Subsequently, the walls of the container were stirred and the mixture was mixed again for another 30 s at high speed (285 ± 10 rpm). The workable pastes obtained were poured into stainless steel molds to obtain prismatic samples ($1 \times 1 \times 6$ $cm^3$) and subjected to 60 strokes on a Proeti shaking table to eliminate bubbles and achieve better compaction of the material. Then, the samples were covered with film to prevent the evaporation of water and thus allow the initiation of geopolymeric reactions and cured at room temperature. After 24 h, they were demoulded and kept at room temperature in a laboratory environment until the day of testing, 7, 28 and 56 days. Details of all prepared samples are given in Table 3 and Fig. 5. For all the mixtures, the liquid/binder ratio selected was 0.45 in order to obtain adequate workability. This value was determined after previous analyzes and ensured good mixing and molding conditions. The samples are designated as *x*CDW-*y*CHM-*z* where × is the CDW precursor content, *y* the CHM precursor content and *z* indicates the activator module of the activating solution (Ms = $SiO_2/Na_2O$). The molar ratio of alkali activated cements can be observed in Table 4.

## 2.3. Characterization of the alkaline activation cements

The ATR-FTIR, XRD was applied to powder pastes (≤100 μm) and SEM-EDS analysis to small pieces of binder using the same equipment and operating conditions as for the raw materials.

Flexural and compressive strength was tested according to UNE-EN 1015-11:2000/A1:2007 [39]. An MTS Insight 5 machine (5 kN capacity) with a displacement speed of 1.0 mm/min was used to determine the flexural strength. Five samples of 60x10x10 mm were tested to determine the average value of the flexural strength. A universal testing machine MTS 8101 (100 kN) with a displacement speed of 2 mm/min was used to determine the compressive strength. Five halves from the flexural test are used to obtain the average value of the compressive strength. A holder is used to apply force to a sample surface of 10 mm x 10 mm.The resulting five halves are used for the bulk density test, through which it is obtained the water absorption and apparent porosity. These tests were determined according to the Archimedes principle following the UNE-EN 1015 10:2000 standard [40].

The specimens were oven dried at a temperature of 100 °C to constant mass. The dry weight (md) is noted. They are then immersed in water until saturation. Subsequently, the specimens are thought in a hydrostatic balance, under water, obtaining the weight (mh) and, finally, the specimen is superficially dried with a wet cloth and the mass of the specimen saturated with water (ms) is determined.

The bulk density (BD), apparent porosity (AP) and water absorption (WA) are obtained according to equations (1)–(3).

$$BD = \frac{md}{m_s - m_h} * \rho_{rh} \quad \text{Eq. (1)}$$

$$WA = \frac{m_d}{m_s - m_d} * 100 \quad \text{Eq. (2)}$$

$$AP = \frac{ms - md}{m_s - m_h} * 100 \quad \text{Eq.(3)}$$

Where:

- $m_d$: is the mass of the dry specimen, in grams.
- $m_h$: is the mass of the specimen immersed in water, in grams.
- $m_s$: is the mass of the saturated specimen, in grams.

**Table 3**
Mix compositions of alkali-activated cements.

| Mixture | CDW (g) | CHM (g) | Sodium silicate (g) | NaOH (g) | $H_2O$ (g) | Liquid/Binder ratio | Ms |
|---|---|---|---|---|---|---|---|
| **100CDW-1.0** | 400 | - | 90.00 | 22.15 | 67.85 | 0.45 | 1.0 |
| **90CDW-10CHM-1.0** | 360 | 40 | 90.00 | 22.15 | 67.85 | 0.45 | 1.0 |
| **80CDW-20CHM-1.0** | 320 | 80 | 90.00 | 22.15 | 67.85 | 0.45 | 1.0 |
| **70CDW-30CHM-1.0** | 280 | 120 | 90.00 | 22.15 | 67.85 | 0.45 | 1.0 |
| **60CDW-40CHM-1.0** | 240 | 160 | 90.00 | 22.15 | 67.85 | 0.45 | 1.0 |
| **100CDW-0.5** | 400 | - | 45.00 | 33.23 | 101.77 | 0.45 | 0.5 |
| **100CDW-2.0** | 400 | - | 135.00 | 11.08 | 33.92 | 0.45 | 2.0 |
| **60CDW-40CHM-0.5** | 240 | 160 | 45.00 | 33.23 | 101.77 | 0.45 | 0.5 |
| **60CDW-40CHM-2.0** | 240 | 160 | 135.00 | 11.08 | 33.92 | 0.45 | 2.0 |

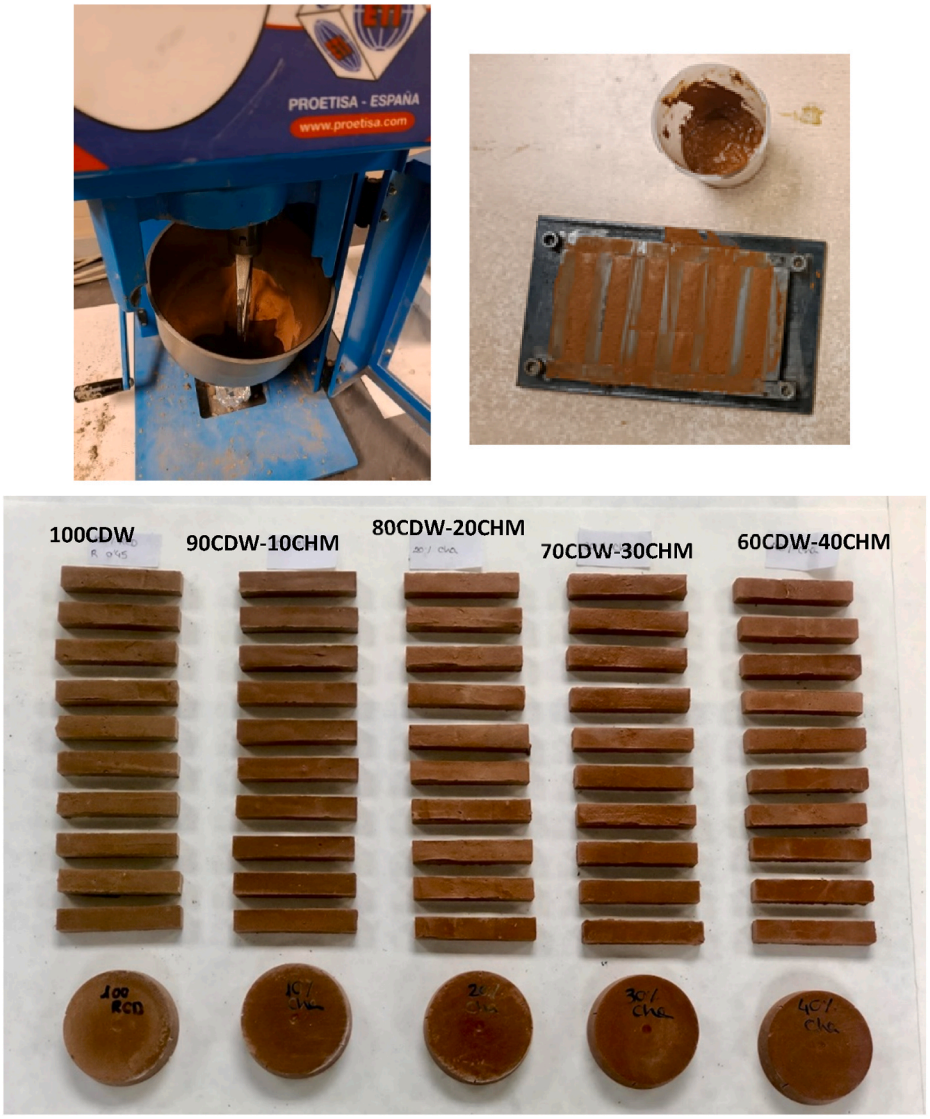


**Fig. 5.** (a) mixing; (b) paste in 60x10x10 mm stainless steel molds and 55 mm diameter cylindrical plastic molds and (c) demolded AACs.

**Table 4**
Molar relation of alkali-activated cements.

| Mixture | Si/Al | Ca/Si | Na/Si |
|---|---|---|---|
| **100CDW-1.0** | 8.34 | 0.34 | 0.22 |
| **90CDW-10CHM-1.0** | 7.70 | 0.30 | 0.26 |
| **80CDW-20CHM-1.0** | 7.17 | 0.27 | 0.29 |
| **70CDW-30CHM-1.0** | 6.73 | 0.23 | 0.32 |
| **60CDW-40CHM-1.0** | 6.35 | 0.19 | 0.35 |
| **100CDW-0.5** | 7.87 | 0.36 | 0.27 |
| **100CDW-2.0** | 8.81 | 0.32 | 0.18 |
| **60CDW-40CHM-0.5** | 6.02 | 0.20 | 0.40 |
| **60CDW-40CHM-2.0** | 6.68 | 0.18 | 0.30 |

- $\rho_{rh}$: density of distilled water, 1000 g/cm$^3$.

The true density of the alkaline activated cements was determined by pycnometry using ethanol as solvent following the UNE-EN 1015 standard [40].

The total porosity of the geopolymers was obtained from the ratio between the bulk density and the true density with Eq. (1).

$$Total\ porosity\ (\%) = \left(1 - \frac{bulk\ density}{true\ density}\right) x\ 1000 \quad \text{Eq. 4}$$

Finally, the thermal conductivity of two samples of 55 mm diameter and 15 mm thick specimens after 28 days of curing was determined according to ISO 8302 [41], using a FOX 50 TA instruments heat flow meter.

## 3. Results and discussion

### 3.1. Physical properties of alkaline-activated cements

As can be seen in Table 5, the addition of CHM ceramic residue does not produce changes in the physical properties, obtaining very similar results for bulk density, water absorption, apparent porosity and total porosity. For example, the bulk density of the control mix, 100CDW-1.0, is 1851 kg/m$^3$ after 28 days of curing, while the bulk density of the 60CDW-40CHM-1.0 mix is 1848 kg/m$^3$, so the substitution of CDW for CHM results in cements with the same physical properties. This may be due to the high similarity between the real densities of the raw materials, being 2677 kg/m$^3$ and 2721 kg/m$^3$ for CDW and CHM residues respectively. However, the influence of curing time is noticeable with an increase in bulk density and a decrease in water absorption, bulk porosity and total porosity. For example, the bulk porosity of the 60CDW-40CHM-1.0 mix is 20.8 %–18.3 % and 15.0 % and the total porosity is 28.4, 24.0 and 21.6 % after 7, 28 and 56 days of curing respectively. The difference in apparent and total porosity values indicates that both open and interconnected pores and closed and inaccessible pores are formed in the alkaline activated cements. The porosity of the mixtures is associated with gel formation and also with the presence of water in the capillaries that are not filled by the alkaline reaction products. The more the material reacts, the more hydration products are formed which fill the pores and densify the binder. Therefore, with the curing time there is a progress of the alkaline activation reaction resulting in a higher amount of cementitious products C-A-S-H gels, and hybrid gel (N,C-A-S-H). Therefore, as the curing reactions take place, most of the CDW and CHM particles react to form denser products, with a consequent decrease in water absorption and porosity [42].

Table 6 shows that the bulk density of control and 60CDW-40CHM AACs increases as the sodium silicate content in the alkaline activator increases, i.e. as the activator modulus Ms increases. This increase is more pronounced when the activator modulus is increased from 0.5 to 1.0, however, a further increase to 2.0 results in similar bulk densities. Thus, the bulk density increases from 1636 kg/m$^3$ (Ms = 0.5) to 1851 kg/m$^3$ (Ms = 1.0) for the 100CDW mix and from 1601 kg/m$^3$ (Ms = 0.5) to 1848 kg/m$^3$ (Ms = 1) for the 60CDW-40CHM mix, for a curing time of 28 days. A low activator modulus (Ms = 0.5) indicates a low degree of reaction, resulting in a low amount of hydration products. A further increase from Ms = 1.0 to Ms = 2.0 produces no improvement in the bulk density of the AACs, giving a bulk density of 1841 kg/m$^3$ at Ms = 2.0 for the 100CDW mix, while the 60CDW-40CHM mix gives bulk densities of 1856 kg/m$^3$ at Ms = 2.0, both at 28 days of curing. By increasing the modulus of the activator from 1.0 to 2.0 even though the sodium silicate content is being increased, the excess of activator may no longer produce improvements in the structures of the AACs, and may even be unfavourable for the formation of the structure.

Water absorption is directly associated with the bulk porosity of the material, and both properties, as well as total porosity, follow a trend opposite to bulk density, since a higher bulk density tends to produce a smaller number of pores, with a consequent decrease in water absorption and vice versa. Therefore, a pronounced decrease in water absorption, apparent porosity and total porosity is observed when Ms is increased from 0.5 to 1.0, indicating a higher amount of reaction products. However, increasing the activator modulus up to 2.0 produces similar or even slightly higher values. Therefore, these data indicate that excessive activator modulus (Ms = 2.0) is no longer beneficial.

The thermal conductivity data of the alkaline activated cements as a function of CHM content after 28 days of curing can be seen in Table 5. The thermal conductivity of the control mix, 100CDW-1.0 is 0.49W/mK, decreasing progressively with the introduction of increasing amounts of chamotte down to 0.38 W/mK for the alkaline activated cement resulting from the 60CDW-40CHM-1.0 mix. The thermal conductivity has a direct relationship with the bulk density. The presence of pores in the specimens affects the rate of heat transfer diffusion, due to the damping in the lattice vibration. Therefore, as porosity in mixtures increases, heat transfer is restricted, which would result in lower thermal conductivity [42]. Since the bulk density is similar for all mixtures, although the water absorption

**Table 5**
Bulk density, water absorption, apparent porosity, total porosity and thermal conductivity as function of the addition of chamotte and curing time for the alkaline-activated cements.

| Physical properties | Curing time (days) | 100CDW-1.0 | 90CDW-10CHM-1.0 | 80CDW-20CHM-1.0 | 70CDW-30CHM-1.0 | 60CDW-40CHM-1.0 |
|---|---|---|---|---|---|---|
| Bulk density (kg/m$^3$) | 7d | 1793 ± 17 | 1774 ± 7 | 1775 ± 16 | 1761 ± 19 | 1803 ± 23 |
| | 28d | 1851 ± 25 | 1841 ± 10 | 1855 ± 17 | 1836 ± 7 | 1848 ± 22 |
| | 56d | 1991 ± 23 | 1897 ± 13 | 1894 ± 8 | 1889 ± 17 | 1901 ± 11 |
| Water absorption (%) | 7d | 10.85 ± 0.36 | 11.54 ± 0.16 | 11.91 ± 0.43 | 11.50 ± 0.59 | 12.40 ± 0.73 |
| | 28d | 9.01 ± 0.50 | 9.52 ± 0.19 | 9.22 ± 0.36 | 9.87 ± 0.55 | 10.04 ± 0.08 |
| | 56d | 6.66 ± 0.44 | 7.07 ± 0.29 | 7.60 ± 0.15 | 7.77 ± 0.14 | 7.89 ± 0.32 |
| Apparent porosity (%) | 7d | 19.5 ± 0.5 | 20.5 ± 0.3 | 21.1 ± 0.6 | 21.9 ± 1.1 | 20.8 ± 0.8 |
| | 28d | 16.7 ± 0.8 | 17.6 ± 0.3 | 17.1 ± 0.5 | 18.5 ± 0.2 | 18.3 ± 0.8 |
| | 56d | 13.3 ± 0.6 | 13.4 ± 0.5 | 13.9 ± 0.2 | 14.7 ± 0.1 | 15.0 ± 0.5 |
| Total porosity (%) | 7d | 29.2 ± 0.4 | 30.5 ± 0.7 | 30.2 ± 0.6 | 30.1 ± 0.4 | 28.4 ± 0.6 |
| | 28d | 25.6 ± 0.6 | 25.1 ± 0.4 | 25.9 ± 0.3 | 25.0 ± 0.5 | 24.0 ± 0.3 |
| | 56d | 24.3 ± 0.5 | 23.1 ± 0.5 | 22.9 ± 0.5 | 22.3 ± 0.5 | 21.6 ± 0.2 |
| Conductivity (W/mK) | 28d | 0.49 ± 0.0 | 0.46 ± 0.0 | 0.41 ± 0.0 | 0.39 ± 0.0 | 0.38 ± 0.0 |

**Table 6**
Bulk density, water absorption, apparent porosity, total porosity and thermal conductivity as function of the activator module and curing time for 100CDW and 60CDW-40CHM AACs.

| Physical properties | Curing time (days) | 100CDW-0.5 | 100CDW-1.0 | 100CDW-2.0 | 60CDW-40CHM-0.5 | 60CDW-40CHM-1.0 | 60CDW-40CHM-2.0 |
|---|---|---|---|---|---|---|---|
| Bulk density (kg/m$^3$) | 7d | 1554 ± 11 | 1793 ± 17 | 1846 ± 16 | 1514 ± 26 | 1803 ± 23 | 1809 ± 10 |
| | 28d | 1638 ± 35 | 1851 ± 25 | 1841 ± 66 | 1601 ± 11 | 1848 ± 22 | 1856 ± 18 |
| | 56d | 1658 ± 7 | 1991 ± 23 | 1913 ± 18 | 1626 ± 28 | 1901 ± 11 | 1881 ± 31 |
| Water absorption (%) | 7d | 18.72 ± 0.50 | 10.85 ± 0.36 | 9.70 ± 0.37 | 20.94 ± 1.28 | 12.40 ± 0.73 | 10.75 ± 0.31 |
| | 28d | 15.96 ± 0.33 | 9.01 ± 0.50 | 9.73 ± 0.68 | 18.03 ± 0.25 | 10.04 ± 0.08 | 10.68 ± 0.19 |
| | 56d | 15.17 ± 0.40 | 6.66 ± 0.44 | 7.28 ± 0.62 | 15.71 ± 0.26 | 7.89 ± 0.32 | 8.17 ± 0.18 |
| Apparent porosity (%) | 7d | 29.1 ± 0.6 | 19.5 ± 0.5 | 17.9 ± 0.6 | 31.8 ± 0.8 | 20.8 ± 0.8 | 19.5 ± 0.5 |
| | 28d | 26.2 ± 0.6 | 16.7 ± 0.8 | 18.5 ± 0.8 | 28.9 ± 0.2 | 18.3 ± 0.8 | 18.0 ± 0.2 |
| | 56d | 25.2 ± 0.6 | 13.3 ± 0.6 | 14.0 ± 1.1 | 25.6 ± 0.2 | 15.0 ± 0.5 | 15.4 ± 0.2 |
| Total porosity (%) | 7d | 36.9 ± 0.4 | 29.2 ± 0.4 | 25.7 ± 0.3 | 40.4 ± 0.8 | 28.4 ± 0.4 | 26.7 ± 0.6 |
| | 28d | 32.7 ± 0.6 | 26.6 ± 0.6 | 21.6 ± 0.5 | 31.9 ± 0.7 | 24.0 ± 0.5 | 23.7 ± 0.3 |
| | 56d | 31.2 ± 0.5 | 25.6 ± 0.5 | 18.6 ± 0.4 | 30.9 ± 0.5 | 21.6 ± 0.5 | 20.2 ± 0.5 |
| Conductivity (W/mK) | 28d | - | 0.58 ± 0.0 | 0.49 ± 0.0 | - | 0.52 ± 0.0 | 0.43 ± 0.0 |

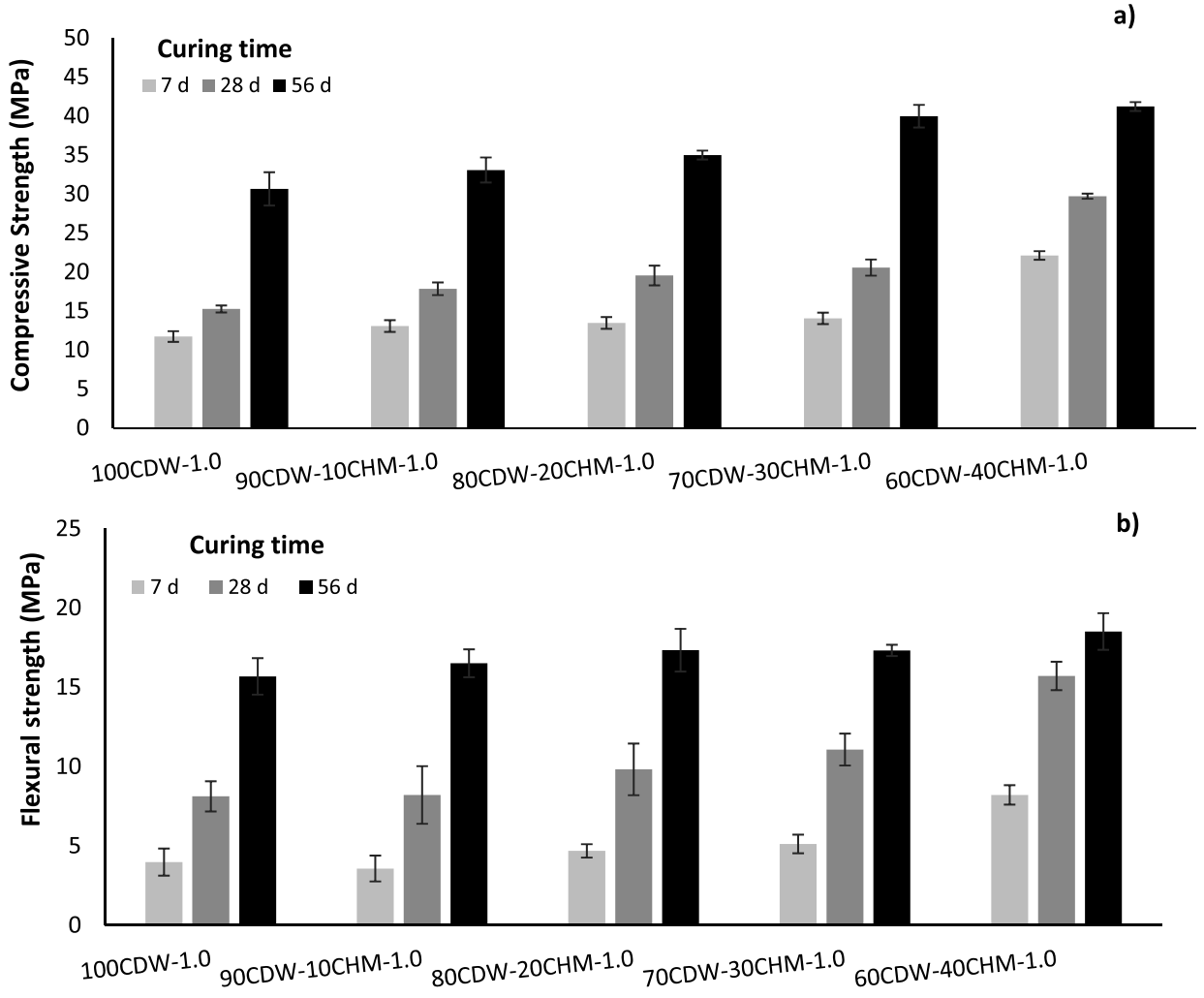


**Fig. 6.** Mechanical properties of alkaline-activated cements with the addition of chamotte a) Compressive strength and b) Flexural strength.

slightly increases with CHM content after 28 days of curing, the open pores would lead to an increase in thermal conductivity. However, these data indicate that thermal conductivity is further influenced by other factors, such as phase composition [43]. Therefore, this different behaviour means that the hydration compounds formed are different, as indicated by SEM micrographs. AACs with a lower amount of chamotte, where there is a higher number of unreacted particles, and a higher amount of unreacted silicon which is a good conductor [44], exhibit higher thermal conductivities. Generally, Na-activated geopolymers show thermal conductivity in the range of 0.65-0.95 W/mK [45]. In general, the geopolymers obtained in this research have lower thermal conductivity (<0.50 W/mK) because the alkaline activation reaction results in polyoxalates with amorphous structure and interconnected pores that provide a tortuous path for thermal gradient flow, thus, the amorphous structure of alkaline activated cement restricts heat transfer [21]. The addition of chamotte could lead to increased microstructural interconnectivity induced by the nucleation of hydration products that could act as insulating barriers resulting in specimens with lower thermal conductivity [46]. Regarding the influence of the activator modulus on the thermal conductivity (Table 6), in the specimens manufactured with an activator with low modulus, Ms = 0.5, this measurement could not be carried out, as the specimens for this test showed a large amount of efflorescence as well as a very slight cohesion, which produced a high fragility and their breakage when introduced into the test equipment, with the consequent impossibility of obtaining a conductivity measurement. Higher conductivities were observed when using an activator modulus Ms = 1.0 with thermal conductivities of 0.58 W/mK and 0.52 W/mK for 100CDW-1.0 and 60CDW-40CHM-1.0 cements after 28 days of curing. The thermal conductivity was reduced to 0.49 W/mK and 0.43 W/mK, respectively, when the activator modulus was increased to 2.0. The introduction of quantities of sodium silicate results in a more interconnected microstructure and a proportional decrease in the overall porosity of the samples. Consequently, as the sample becomes more interconnected, there are fewer pores present to disturb the flow of thermal energy, which favours thermal conductivity. In addition, the presence of more drying shrinkage cracks as the activator modulus increases can lead to a higher insulating capacity. Also, the higher insulating capacity of cements with excess sodium silicate may be due to the weak reactions between the activator and precursors, which would generate thermally resistant interface layers between the gels and unreacted particles, which could also help to reduce the thermal conductivity of AACs [47].

### 3.2. Mechanical properties of alkaline-activated cements

The compressive strength of the 100CDW-1.0 control cement is 15.2 and 30.7 MPa at 28 and 56 days of curing, respectively (Fig. 6a). The addition of increasing amounts of CHM resulted in a gradual increase in compressive strength obtaining values of 17.8 and 33.1 MPa, 19.5 and 35.0 MPa, 20.5 and 40.0 MPa and 29.7 and 41.3 MPa at 28 and 56 days of curing, respectively with the addition of 10 wt%, 20 wt%, 30 wt% and 40 wt% CHM, respectively (Fig. 6a). The flexural strength (Fig. 6b) follows the same trend as the compressive strength, increasing progressively as increasing amounts of CHA are incorporated with values from 8.1 to 15.7 MPa with the control mix (100CDW-1.0) to 15.7 and 18.5 MPa with the maximum amount of CHM (60CDW-40CHM-1.0) after 28 and 56 days of curing respectively. In all alkaline activated cements, the same liquid/binder ratio, the same activator modulus and the same curing temperature have been used, so that the mechanical strength will depend fundamentally on the amount and type of gel formed, which in turn depends, to a large extent, on the chemical composition of the precursors, as well as on the molar ratios obtained in each mixture.

An increase in mechanical strength is observed with decreasing Si/Al and Ca/Si molar ratios (Table 4). This may be due to the fact that the $Ca^{2+}$, $Si^{4+}$ and $Al^{3+}$ ion ratios are not adequate, being very high when high amounts of CDW are used, thus producing an imbalance in the network. This implies that the high initial ion concentration may have slowed down or stopped the reaction of the precursor by preventing its interaction with the alkaline solution or by creating separate composite gels [48]. Therefore, the use of CDW results in AACs with lower mechanical strengths due to the lower reactivity of the precursor with respect to the CHM residue. In addition, its high CaO content generally consumes alkalis from the activator, slowing down the dissolution and polymerization processes and generating $Ca(OH)_2$ [23,49,50]. The latter is prone to carbonation, which results in a decrease of the strong Si-O-Al bonding in the geopolymeric system and therefore generates binders with higher brittleness. Also, the CDW residue possesses a lower amount of alumina which plays an essential role in the development of metastable Al-O-Si bonds at early reaction times and their conversion to stable forms at advanced stages of geopolymerisation [48]. Therefore, a very high Si/Al ratio results in a very slow alumina release rate, which can be attributed to the lower availability of aluminium for gel formation [23]. The addition of CHM, richer in soluble $Al_2O_3$, provides the necessary amount of aluminosilicates of amorphous structure to favour the stages of dissolution, nucleation, condensation, and reorganization of the geopolymerisation products [13,16]. In addition, the Na/Si ratio (Table 4) also influences the mechanical properties. Increasing the Na/Si ratio with the incorporation of increasing amounts of CHM can provide more $Na^+$ cations, which are necessary for the solubility of aluminosilicates and the charge equilibrium of silica species, thus facilitating a more uniform development of the more stable microstructure. Therefore, increasing $Na^+$ ions can promote electrostatic attraction and charge neutralisation, which can also accelerate the dissolution and polymerization processes [51]. The increased $Na^+$ concentration plays an important role in stimulating the movement of silicate species (Si-O-), which may have boosted particle bonding and triggered an enhanced mechanical response [48]. Therefore, the decrease in Si/Al molar ratio from 8.34 to 6.34 and the increase in Na/Si molar ratio from 0.22 to 0.35 from the control specimen (100CDW-1.0) to the 60CDW-40CHM-1.0 resulted in an increase in compressive strength possibly due to the fact that in these cements there is a more adequate supply of soluble silica, a more appropriate level of alkalinity, and relevant charge-balanced $Na^+$ cations in the alkali-activated cement matrix, thus initiating greater silica-aluminate separation and better formation of reaction products [48].

Regarding the influence of the chemical composition of the raw materials, on the one hand, the CDW precursor is mainly composed of $SiO_2$ (51.69 wt%) with a high amount of CaO (18.93 wt%) and a low amount of $Al_2O_3$ (5.93 wt%) (Table 2). Whereas, the CHM precursor y, which partially replaces CDW, contains higher amounts of $Al_2O_3$ (12.11 wt%) and much lower proportions of CaO (8.67

wt%) also feel the majority compound $SiO_2$ content (63.08 wt%) [51]. In addition, the CDW contains a significant organic matter content, as indicated by the LOI value (15.54 wt%), which may limit its reactive potential. The residual carbon could behave as an alkali sink and adsorb alkaline cations [52] reducing the polycondensation reaction, increasing the setting time with a consequent loss of mechanical strength [50]. In the control mixture (100CDW-1.0), a large amount of C-A-S-H gel is formed in the early stages of the alkaline activation reactions, together with smaller amounts of N-A-S-H gel, as indicated by SEM micrographs and EDS analysis (Fig. 12). With the progressive addition of CHM and the consequent decrease of CDW (90CDW-10CHM-1.0, 80CDW-20CHM-1.0 and 70CDW-30CHM-1.0), there is an increasing increase of available $Al^{3+}$, while the amount of $Ca^{2+}$ decreases. Therefore, a partial substitution of $Na^{+}$ ions by the higher-valent $Ca^{2+}$ ion may take place in the predominant N-A-S-H gel, which would modify the N-A-S-H gel without totally degrading it, favouring the formation of a gel with a hybrid microstructure of the (C,N)-A-S-H type [53,54]. The latter can improve the stiffness of alkali-activated cements, especially at room temperature [10,33] and has a positive effect on the mechanical strength [55]. The gel will become richer in aluminates as the CHM content increases. Therefore, the addition of increasing amounts of CHM will result in the Si/Al and Na/Si molar ratios becoming more and more balanced, providing sufficient $OH^{-}$ and $Na^{+}$ contents that can lead to better cleavage of bonds such as Si-O-Si, Al-O-Si, Al-O- Al and Ca-O. Therefore, it would lead to the formation of lesser amount of C-A-S-H gel, more amount of amorphous N-A-S-H gel, as well as, a combination of both (C,N)-A-S-H [33]. Therefore, the increase of mechanical strengths in alkaline activated cements containing up to 40 wt% CHM (60CDW-40CHM-1.0), can be attributed to the coexistence of C-A-S-H gel whose presence is decreasing with increasing percentage of CHM replacing CDW, together with mixed (C,N)-A-S-H gel.

The compressive and flexural strengths increase significantly when the activator modulus is increased from 0.5 to 1.0 with flexural and compressive strengths after 56 days of curing of 1.4 and 5.7 MPa and 16.5 and 30.6 MPa for 100CDW-0.5 and 100CDW-1.0 cements, respectively (Fig. 7). These values increase to 3.5 and 6.6 MPa for the 60CDW-40CHM-0.5 specimens and to 18.5 and 41.2 MPa for the 60CDW-40CHM-1.0 cements. However, further increases in the activator modulus Ms = 2.0 result in a slight decrease in flexural and compressive strength.

The lowest mechanical strengths are obtained for an activator modulus Ms = 0.5. This is mainly due to the inadequate soluble silica

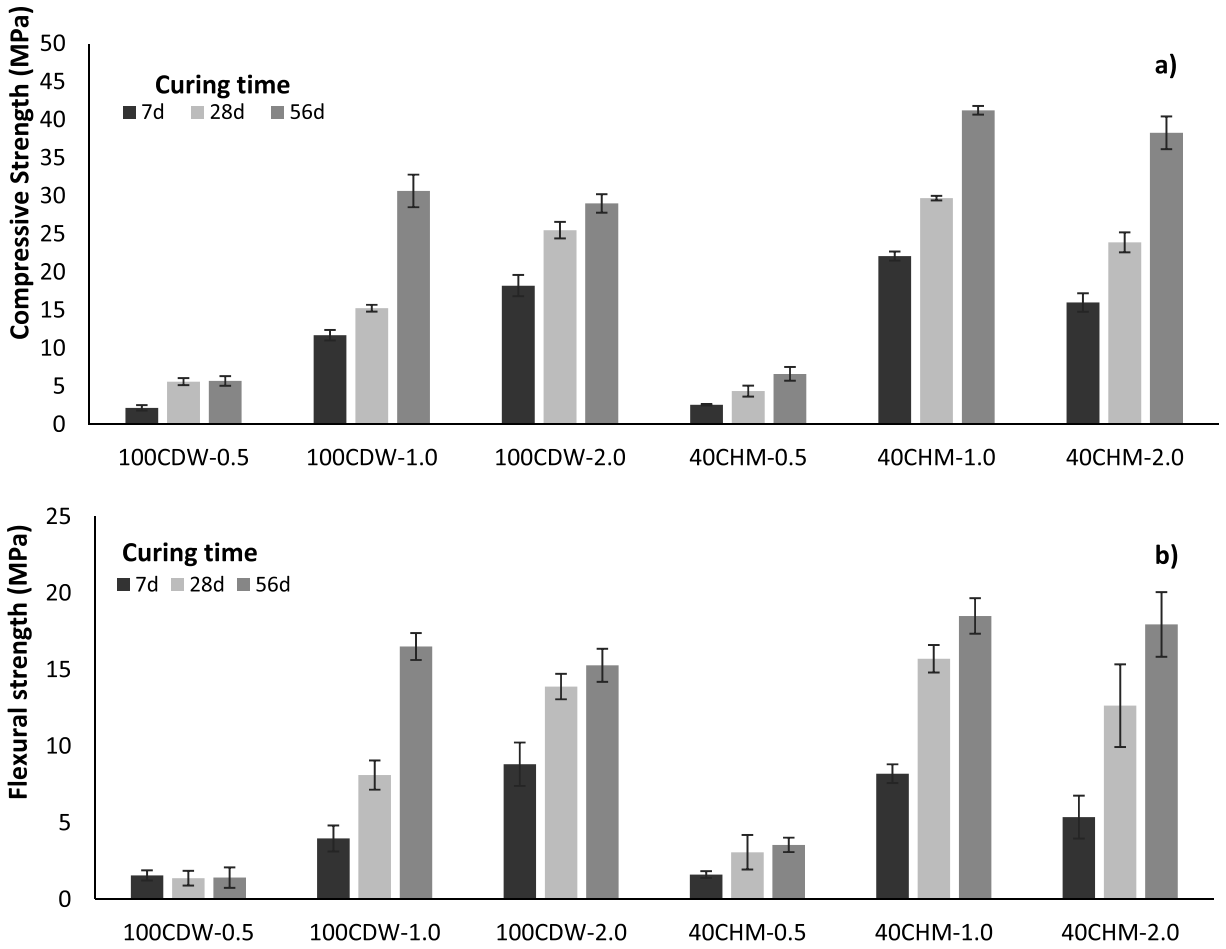


**Fig. 7.** Mechanical properties of alkaline-activated cements 100CDW and 60CDW-40CHM with Ms = 0.5, 1.0 and 2.0, a) Compressive strength and b) Flexural strength.

provided by the low silicate modulus for the polymerization reaction with $Ca^{2+}$ and $Al^{3+}$ in the liquid phase [56] which leads to low strengths of alkali-activated cements due to a not fully mature molecular structure caused by incomplete dissolution of aluminosilicates. This causes deterioration of the microstructure leading to increased porosity as well as increased pore size [48,57]. This increase in porosity may also be due to the release of physically bound water not consumed due to the low level of geopolymerisation. In addition, the excess $Na^{+}$ that remains unreacted in the matrix of alkaline activated cements after equilibration of Si and Al tetrahedra can leach out or lead to efflorescence formation due to the accumulation of carbonated sodium oxide on the surface of the material [9, 51,58]. On the contrary, an excessive $Na_2SiO_3$ content and a NaOH defect in the activator, as occurs when a high activator modulus (Ms = 2.0) is used, causes the alkaline activator solution to become more viscous, this effect decreases the workability of the mixtures and reduces the setting time [27] so that reaction products form rapidly in the highly alkaline medium inhibiting the geopolymerisation reaction. In addition, an excessive amount of $Na_2SiO_3$ can hinder the evaporation of water and the formation of polymerization products during the polycondensation process which could lead to a structure with larger unreacted particles and higher porosity [33,59]. In contrast, with adequate proportions of NaOH and $Na_2SiO_3$, (Ms = 1.0), there is a donation of sufficient

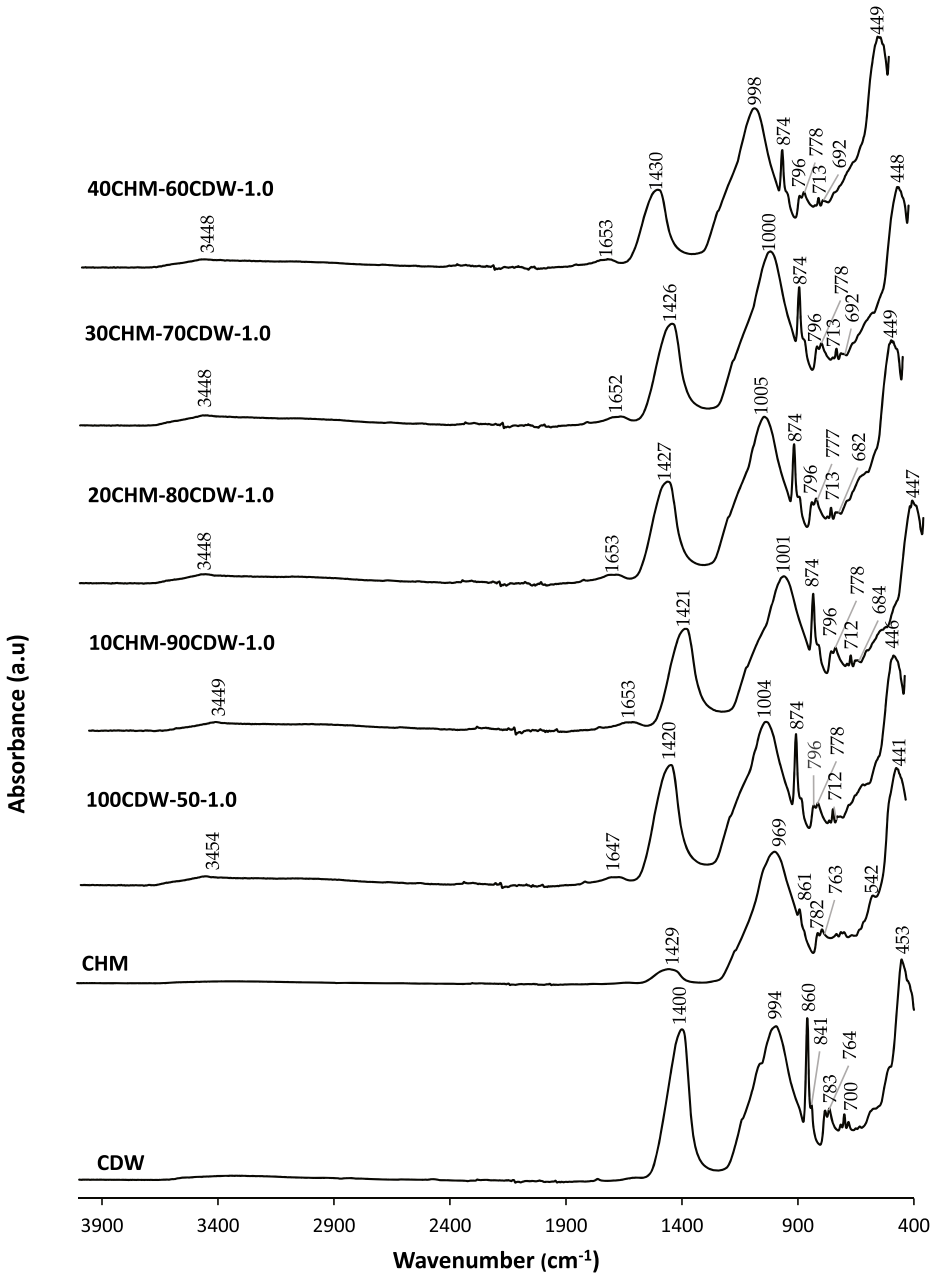


**Fig. 8.** FTIR of alkaline-activated cements with increasing amounts of chamotte and raw materials.

soluble silica species (Si-O) from the sodium silicate agent, therefore, more Si-O-Si bonds are formed which facilitate the right conditions for the formation of a geopolymeric structure [9], creating a stronger material [1]. The $Si^{4+}$ ions provided by the solution can react with the reactive $Si^{4+}$, $Ca^{2+}$ and $Al^{3+}$ species of the precursors, dissolving more particles, leading to a higher formation of reaction products and a higher degree of reaction [16], and a denser microstructure, thus, the porosity is reduced. Furthermore, sodium silicate contributes to a better interface between the non-reactive particles and the gel matrix and, consequently, to a higher mechanical strength of the aluminosilicate gel [16,33,58]. On the other hand, as the sodium silicate solution content in the solution increases, efflorescence is significantly reduced, probably due to the lower content of free sodium as a consequence of a higher degree of geopolymerisation [29].

The flexural and compressive strength of alkaline activated cements increases with curing time. However, this increase is more pronounced at longer curing times, from 28 to 56 days. This increase is attributed to a higher degree of geopolymerisation as the curing time increases, as well as to the quality of the gel formed. These data could indicate that after 28 days of curing, the polycondensation process is not yet virtually complete and there are still raw material particles to be dissolved [60]. That is, the improvement in mechanical strength with curing time occurs mainly because the stages of the alkaline activation process involving gelation and transformation are still occurring [22].

### 3.3. FTIR of alkaline-activated cements

In the process of hardening alkali-activated cements manufactured with CDW and CHM, a series of chemical bonds are formed as a result of the chemical reactions that take place once the activating solution is added to the mixture. Fig. 8 displays the FTIR spectra of alkali-activated cements after 28 days of curing, as a function of the incorporated CHM content. For comparison, the FTIR spectra of the raw materials CDW and CHM are also presented. Table 7 displays the assignment of vibrational frequencies of the AACs.

The bands centered around 3450 $cm^{-1}$ and 1650 $cm^{-1}$ are assigned to the stretching vibrations of the -OH bond and the bending vibrations of H-O-H in the bound water molecules, respectively. These bands originate from water molecules adsorbed on the surface or trapped in cavities within the structures of alkali-activated cements [50,54,55]. The higher intensity of both bands with larger amounts of CDW can be attributed to the greater quantity of water molecules present in the alkali-activated cement as the Si/Al ratio increases, as well as to a lower degree of geopolymerization reaction for higher CDW contents [60]. The band centered around 1425 $cm^{-1}$ is assigned to the asymmetric stretching vibrations of the C-O bonds. This band, along with another band centered at approximately 870 $cm^{-1}$ corresponding to the symmetric deformation vibration of the O—C—O bonds, indicates the presence of carbonates $(CO_3)^{-2}$. Both bands intensify in AACs with higher CDW content, indicating that the excess calcium in the precursor leads to the formation of a greater amount of carbonates due to increased $Ca(OH)_2$ formation, which reacts with environmental $CO_2$ [21,50,60] according to XRD data (Fig. 10). The last band assigned to the C-O bond vibrations in carbonate groups appears centered at approximately 712 $cm^{-1}$ [7,50]. The main band, which is the fingerprint of the geopolymerization process [42], appears centered at approximately 1000 $cm^{-1}$. This band is attributed to the asymmetric stretching vibration of the Si-O-Si and Si-O-A bonds [10,30]. A shift of this band towards lower wavenumbers is observed with the incorporation of CHM, as this band in the precursor is centered at lower wavenumbers, 969 $cm^{-1}$. This displacement can be associated with the dissolution of the aluminosilicate source and is indicative of the enhanced formation of C-A-S-H and/or N-A-S-H gels during the alkali activation process of alkali-activated cements [10,53,54]. For the CDW precursor, the carbon content can absorb some of the alkalis needed for the reorganization and cross-linking of leached Si, Al, and Ca species to form gel, resulting in reduced polymerization and lower strength properties [30]. In cements with high CDW content, the presence of $Ca^{2+}$ in the solution favors the formation of C-A-S-H type gels as can be observed in SEM-EDS analysis (Fig. 12). As the calcium content is dominant, there may be no additional Si and Al left after the calcium is completely consumed, or the remaining concentrations of Si, Al, and alkalis may not be sufficient to promote the formation of a highly polymerized structure. The use of increasing amounts of CHM promotes the formation of N-A-S-H and hybrid (N,C-A-S-H) type gels as shown in the SEM micrographs (Fig. 13), due to the presence of soluble silica and alumina monomers in the solution at high concentrations, leading to the production of oligomers and subsequent polymerization [61]. In AACs, the double band centered at 796–778 $cm^{-1}$ and the bands centered at approximately 680 $cm^{-1}$ and 447 $cm^{-1}$ are also observed, which also appear in both precursors. The double band can be assigned to the bending of the Si-O-Si bonds in the network of unreacted silica [22,50,55]. While the other two bands are attributed to the bending vibration of the Si-O-Si and Si-O bonds of quartz, respectively [21,42,50], indicating a weak dissolution of quartz phases in an alkaline medium observed in the XRD patterns.

**Table 7**
FTIR spectra band assignments.

| Wavenumber ($cm^{-1}$) | Vibration mode | References |
|---|---|---|
| 3450 | Stretching vibration of the -OH bond | [50,54,55] |
| 1650 | H-O-H bending vibration | [50,54,55] |
| 1425 | Asymmetric stretching vibration of the O-C-O bond | [21,50,60] |
| 1000 | Asymmetric stretching of the Si-O-Si and Al-O-Si groups | [10,30,42] |
| 870 | C-O bond vibrations in carbonate groups | [21,50,60] |
| 796 | Si-O-Si bond bending vibration | [22,50,55] |
| 778 | Si-O-Si bond bending vibration | [22,50,55] |
| 712 | C-O bond vibrations in carbonate groups | [7,50] |
| 680 | Si-O-Si bond bending vibration in quartz | [21,42,50] |
| 447 | Si-O bond bending vibration in quartz | [21,42,50] |

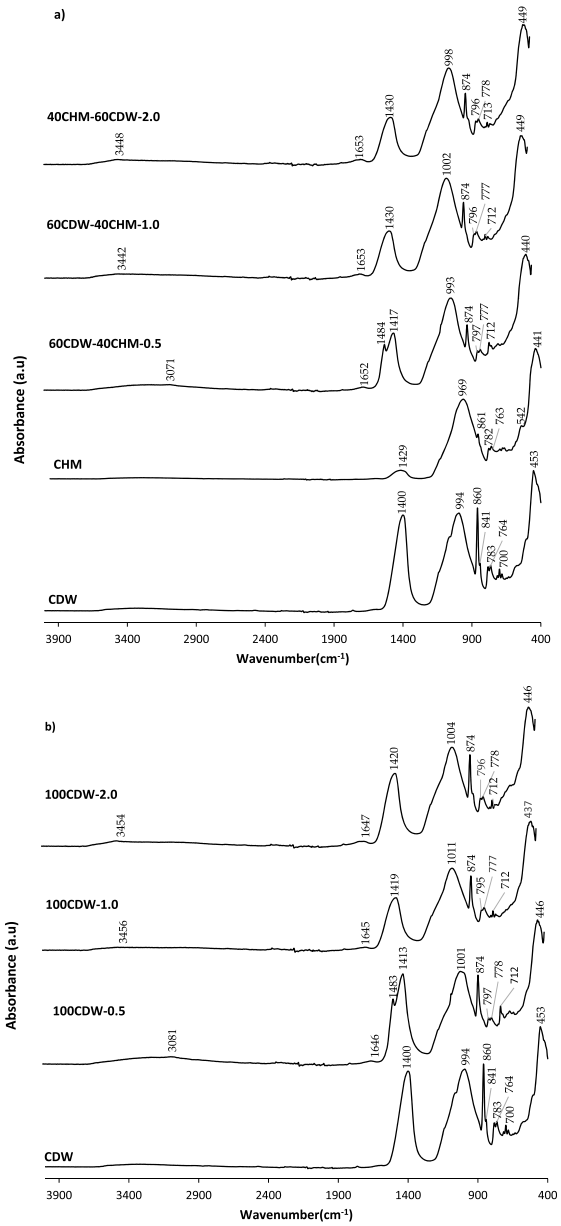


**Fig. 9.** FTIR spectrum of a) 100CDW with Ms = 0.5, 1.0 and 2.0 and b) 60CDW-40CHM with Ms = 0.5, 1.0 and 2.0 at 28 days of curing.

In Fig. 9a, the Fourier-transform infrared spectra of the 100CDW mixture with different activator modules, as well as the spectrum of the CDW raw material, can be observed. Similarly, in Fig. 9b, the Fourier-transform infrared spectra of the 60CDW-40CHM mixtures with different activator modules, along with the spectra of the CDW and CHM raw materials, are shown.

The activator module or silica content of the activating solution influences the shift of the main band associated with Si-O-T (T = Si or Al in tetraedrical position). The mixtures with Ms = 0.5 experienced the smallest shift, obtaining the lowest wavenumber values of 993 and 1001 $cm^{-1}$ for the 100CDW-0.5 and 60CDW-40CHM-0.5 specimens, respectively. The shift towards higher wavenumbers is obtained when using an activator module Ms = 2.0 and primarily for Ms = 1.0. This shift could indicate changes in the degree of polymerization. The increase in the wavenumber indicates a higher degree of polymerized Si-O network, resulting in more highly polymerized gels, as supported by the data on flexural and compressive strength and SEM analysis [61].

The band centered at 1430 $cm^{-1}$ assigned to the stretching vibrations of O-C-O in carbonates undergoes a splitting in AACs with a low activator module (Ms = 0.5). This splitting is indicative of the presence of excess Na, indicating the formation of $Na_2CO_3$, in addition to the formation of $CaCO_3$ [32,37].

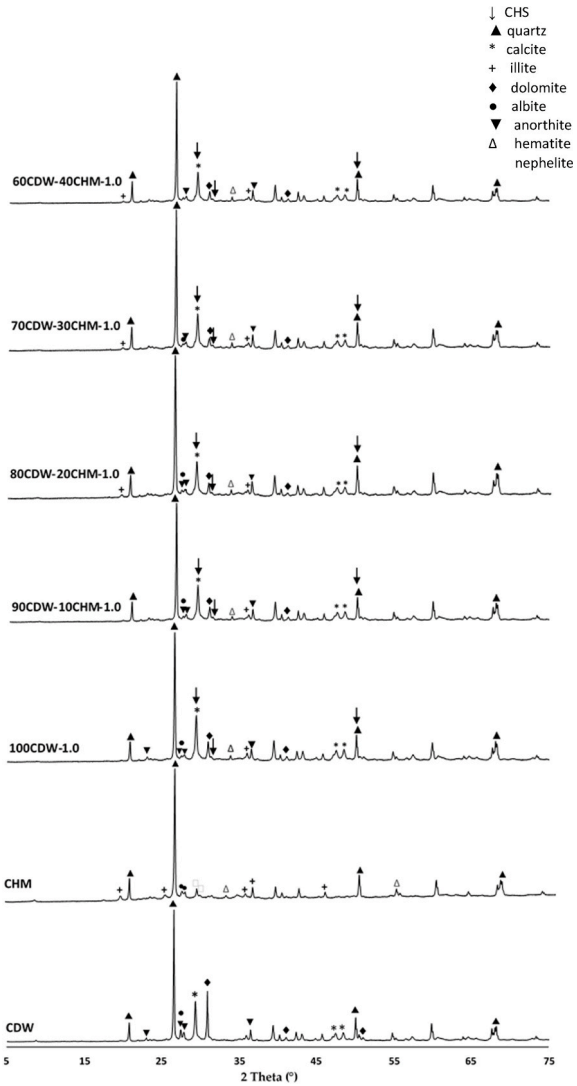


**Fig. 10.** DRX of alkaline-activated cements with increasing amounts of chamotte and raw materials.

### 3.4. DRX of alkaline-activated cements

Fig. 10 displays the X-ray diffractograms of the alkali-activated cements synthesized after 28 days of curing, as a function of the amount of incorporated CHM. The diffractograms of the raw materials, CDW and CHM, are also included for comparison. In all the represented alkali-activated cements, intense diffraction peaks corresponding to the raw materials were observed, such as the peaks related to quartz present in both precursors and calcite present in the CDW residue. This suggests that quartz does not react or only partially reacts during the geopolymerization process as can be seen in the SEM-EDS analysis, indicating a low or negligible reactivity of the crystalline phases. Additionally, less intense diffraction peaks such as anorthite, illite, and albite are observed, indicating that the crystal surface is attacked by the alkaline medium [27,48]. The halo located in the range between 20° and 40° 2θ, which is usually indicative of aluminosilicate gel formation, although weak in all AACs, is slightly more pronounced in samples with increased CHM content, suggesting the presence of a higher relative proportion of geopolymeric gel when larger amounts of CHM were used as a precursor [27]. On the other hand, an intense peak can be observed at approximately 29° 2θ. This diffraction peak may correspond, in addition to calcite, to the formation of new phases developed in mixtures such as calcium silicate hydrate (C-H-S) (PDF 33–0306), 2θ = 29,355°, 32,053°, and 50,077°.

In Fig. 11a, the X-ray diffractograms of the 100CDW mixture with different activator modules, as well as the spectrum of the CDW raw material, can be observed. Similarly, in Fig. 11b, the X-ray diffractograms of the 60CDW-40CHM mixture with different activator modules, along with the diffractograms of the CDW and CHM raw materials, all at 28 days of curing, are shown.

Due to the similarity of the diffractograms of both mixtures with different alkali activator modules, only those diffraction peaks showing some differences with the different alkali activator modules have been marked. In the 100CDW paste, it can be observed that both the diffraction peaks centered at approximately 28° (2θ), corresponding to the feldspars, albite ($NaAlSi_3O_8$), and anorthite

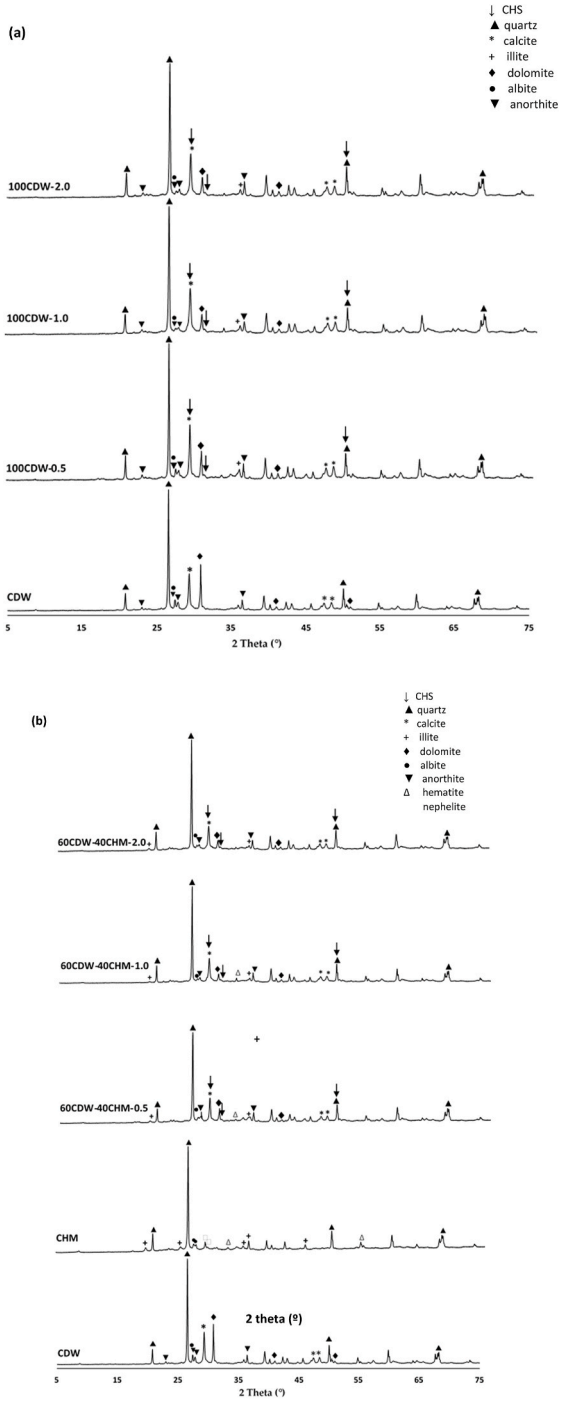


**Fig. 11.** XRD patterns of a) 100CDW with Ms = 0.5, 1.0 and 2.0 and b) 60CDW-40CHM with Ms = 0.5, 1.0 and 2.0 at 28 days of curing.

($CaAl_2Si_2O_8$), as well as the diffraction peak located around 31° (2θ), associated with dolomite ($CaMg(CO_3)_2$) from the limestone, decrease in intensity as the alkali activator module increases. Regarding the 60CDW-40CHM mixture, similar to the previous mixture, the diffraction peak associated with dolomite located around 31° (2θ) decreases in intensity as the alkali activator module (Ms) increases. Meanwhile, the diffraction peaks corresponding to illite (a phyllosilicate) that can be observed near 34.8° (2θ) in the mixture with Ms = 0.5 decreasesr in the mixtures with Ms = 1.0 and 2.0. Indeed, this could demonstrate that as the amount of sodium silicate in the activator increases, there is a higher dissolution of these phases, more amorphousness, and a greater degree of geopolymers formation. Furthermore, the consumption of illite indicates a more extensive formation of N-A-S-H gel, as well as a combination of C-A-S-H and N-A-S-H gel to form a hybrid (C,N)-A-S-H gel [22] according con FTIR and SEM-EDS analysis. This suggests different degrees of

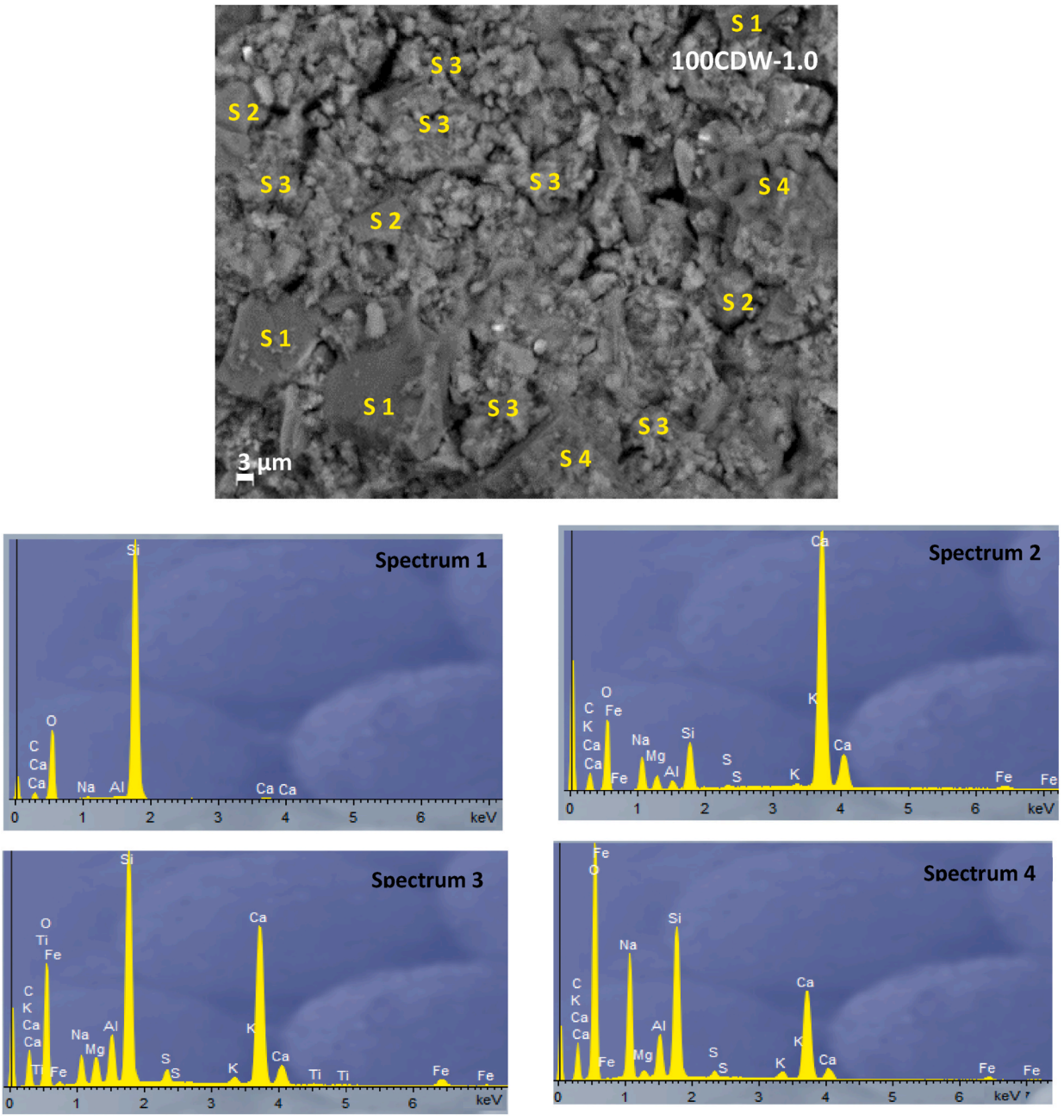


**Fig. 12.** SEM micrographs and EDS analysis of control AACs, 100CDW-1.0 at 1Kx.

geopolymers formation with an increase in the Ms of the alkali solution.

### 3.5. SEM-EDS of alkaline-activated cements

The morphology of the selected alkali-activated cements, control 100CDW, and the optimal sample with higher CHM content, 60CDW-40CHM-1.0, was examined using SEM (Scanning Electron Microscopy). The chemical composition was analyzed using Energy Dispersive X-ray Spectroscopy (EDS).

The control mixture 100CDW-1.0 (Fig. 12) exhibits a non-homogeneous microstructure in which microcracks can be observed, generated both due to material shrinkage and water evaporation, typical of alkali-activated cements with high Si/Al molar ratios. Additionally, the presence of unreacted $SiO_2$ particles embedded in the formed gel can be observed according to XRD and FTIR data. The presence of these particles is confirmed by EDS analysis (Spectrum 1), as well as unreacted Ca-rich CDW particles (Spectrum 2). This indicates poor and/or partial dissolution of the CDW residue, leading to the formation of weak bonding agents between the

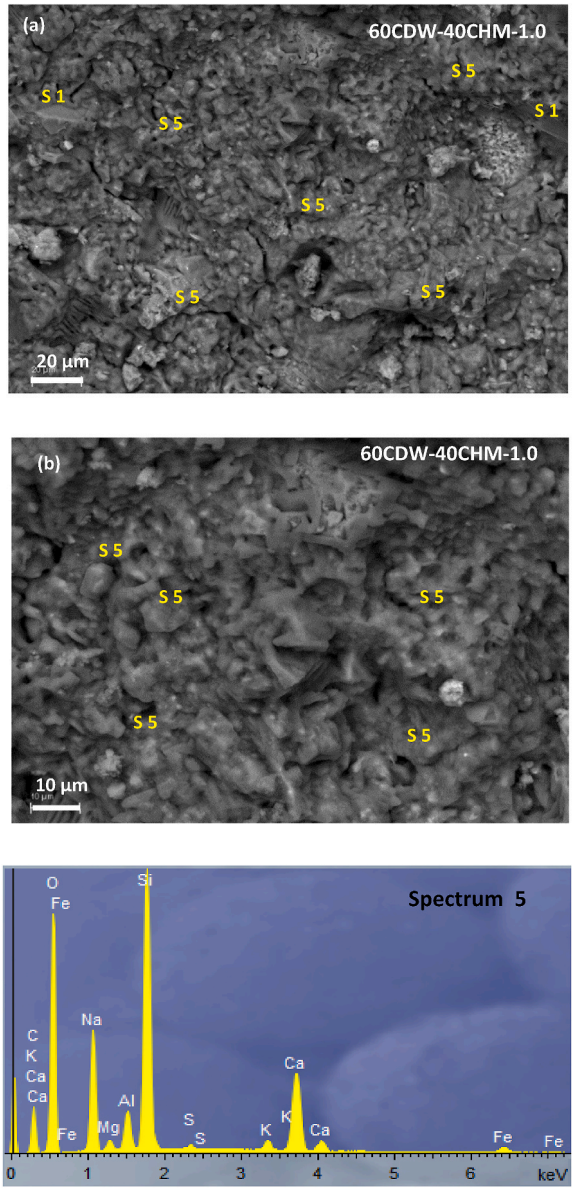


**Fig. 13.** SEM micrographs and EDS analysis of 60CDW-40CHM-1.0 at (a) 500x and (b) 1Kx.

reaction products, consistent with lower mechanical strength.

The predominant formation of calcium aluminosilicate gel (C-A-S-H) can be observed (Spectrum 3), characterized by a region with greater granularity, rich in silicon and calcium, and lower concentrations of aluminum and sodium. Additionally, to a lesser extent, the formation of a more fibrous gel of sodium and calcium aluminosilicate hydrate (N,C-A-S-H) can also be observed (Spectrum 4). The coexistence of both gels results in a weaker structure because these two gels compete to form, leading to a less homogeneous structure due to the separation of both phases and unreacted particles, as indicated by the compressive strength data. Moreover, neither of the phases acts as a microaggregate to fill pores and cracks [23].

The micrograph of the 60CDW-40CHM-1.0 AACs (Fig. 13) shows a more homogeneous microstructure compared to the control mixture, with a lesser amount of unreacted particles, indicating that both precursors have been almost completely dissolved under the alkaline network, which aligns with the better mechanical performance reported for this mixture. However, some microcracks can still be observed.

A predominance of the hybrid gel (N,C-A-S-H) (Spectrum 5) can be observed, with an elemental composition rich in silicon and sodium, and in lesser proportion in calcium and aluminum. This mixed amorphous gel is formed due to the combination of CA-S-H and N-A-S-H gels, being the main product of geopolymerization. The presence of the N,C-A-S-H gel exhibits greater cohesion, providing the 60CDW-40CHM-1.0 cements with a stronger structure and higher compressive and flexural strength compared to the control mixture,

100CDW-1.0, as supported by the flexural and compressive strength data [23].

The SEM-EDS analysis of the 100CDW and 60CDW-40CHM mixtures as a function of the activator module (Fig. 14) indicates that when using a low activator module, Ms = 0.5, both in the 100CDW-0.5 and 60CDW-40CHM mixtures, there is a considerable amount of unreacted or partially reacted particles embedded in the gel. In both cements, unreacted quartz particles (Spectrum 1) as well as unreacted CHM precursor particles rich in calcium (Spectrum 2) can be observed according to XRD and FTIR data. Additionally, excess sodium from the activator can be seen (Spectrum 6), which is not part of the reaction product, the hybrid C,N-A-S-H gel (Spectrum 7 and 8). The use of low activator modules results in AACs with a microstructure characterized by weak compaction, loose morphology, and high porosity, indicating a low degree of reaction in the system with a low formation of the hybrid gel. Furthermore, it can be

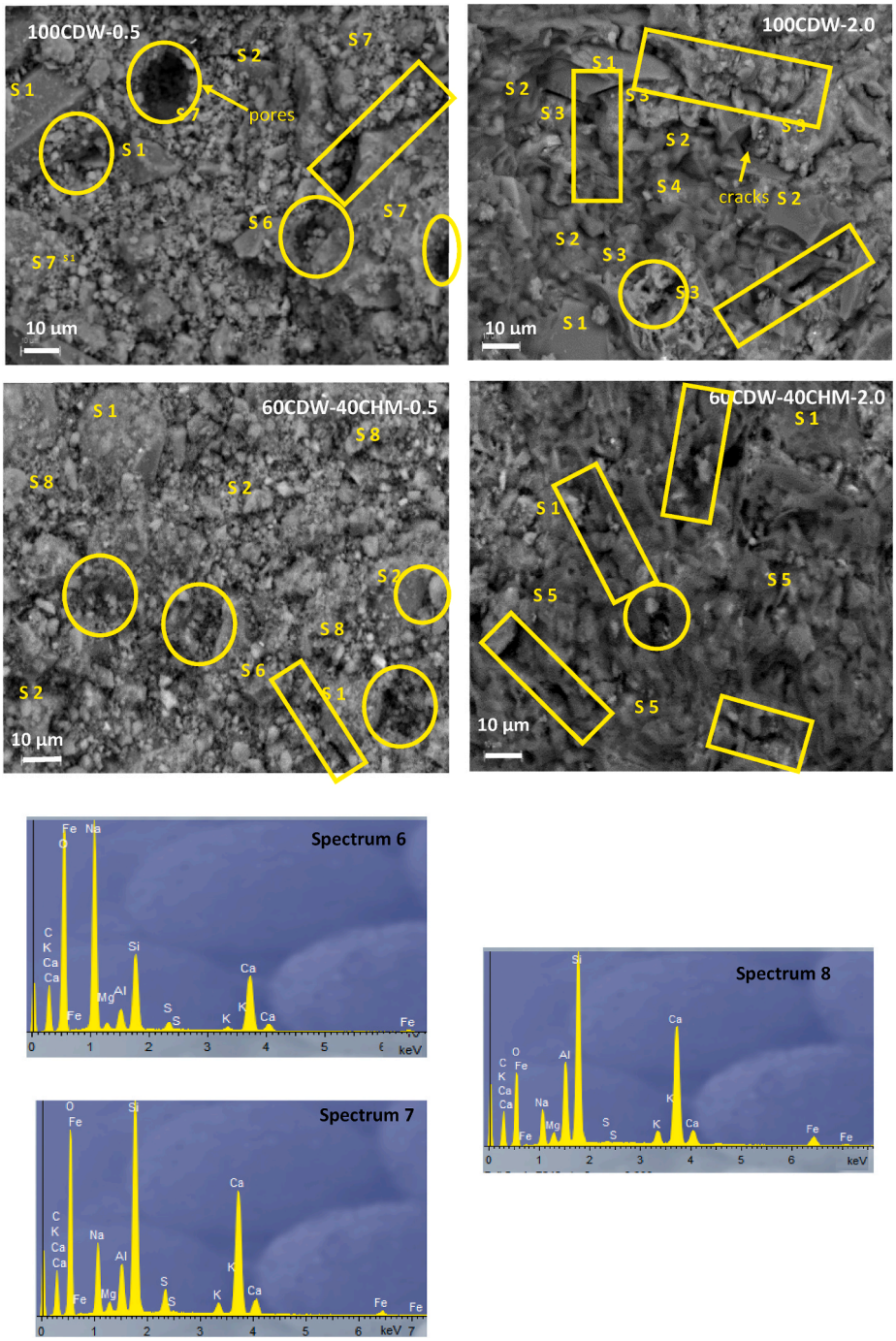


**Fig. 14.** SEM micrographs-EDS analysis of a) 100CDW with Ms = 0.5, and 2.0 and b) 60CDW-40CHM with Ms = 0.5, and 2.0 at 28 days of curing.

observed that the 100CDW-0.5 mixture has a coarser pore size distribution compared to the 60CDW-40CHM-0.5 mixture, resulting in lower mechanical strengths.

By increasing the activator module up to Ms = 1.0 and Ms = 2, a compact material with a denser and more homogeneous structure is observed, exhibiting reduced porosity and pore size, as well as a decreased number of unreacted particles. This observation indicates the formation of more hydration products. In the 60CDW-40CHM specimens, a more fibrous and irregular structure can be observed, primarily corresponding to an amorphous network microstructure of the alkali-activated cement due to the formation of the hybrid N, C-A-S-H gel. This could be because the C-A-S-H gel, with its higher filling capacity, can deposit and fill the porous spaces between particles, forming a denser microstructure and improving the overall physical and mechanical properties. Additionally, this gel combines with the N-A-S-H gel, which is much more significant in this mixture than in the control cements, where it forms only to a lesser extent. This justifies the higher mechanical strength of AACs that incorporate CHM. In samples with a higher activator module, Ms = 2.0, an increase in cracks caused by drying shrinkage during the curing process, lower gel formation, and a higher number of unreacted particles can be observed. This is due to the decrease in the pH of the activator and the presence of an excess of soluble Si in the system. As a result, the particles start to lose cohesion, becoming trapped in the reaction product matrix, leading to reduced dissolution of CDW and CHM particles and a lower amount of available Al to form the corresponding gels. Therefore, increasing Ms beyond a certain value adversely affects the mechanical properties.

## 4. Conclusions

This study investigates the influence of incorporating different amounts of ceramic fraction, chamotte residue (0–40 wt%), and different silicate modules (Ms = 0.5, 1.0, and 2.0) on the microstructural and macroscopic properties of alkali-activated cements (AACs) based on construction and demolition waste with a high fraction of concrete residues. The following conclusions are primarily drawn from this research:

1) The addition of CHM enhances the mechanical properties of AACs based on CDW. The flexural and compressive mechanical strength increases linearly with the incorporation of increasing amounts of chamotte. The most significant improvement is achieved for cements incorporating 40 wt% CHM (60CDW-40CHM-1.0), with flexural and compressive strengths after 56 days of curing reaching 18.5 and 41.2 MPa, respectively, representing an increase of 18.0 % and 34.4 % compared to the control cements (100CDW-1.0). The increase in mechanical strength can be attributed to the different nature of the gel formed according to the data obtained from SEM-EDS analysis.
2) The activator modulus has a great influence on the mechanical properties due to a strong influence on the structure and morphology of the reaction products formed. Thus, when the silicate module of alkali activators increases from 0.5 to 1.0, it leads to a significant upward trend in mechanical properties. However, a further increase to 2.0 causes a slight decrease in the flexural and compressive strength of the AACs.
3) The use of low Ms values results in low dissolution of the precursors, leading to a porous and poorly packed microstructure with a large number of unreacted particles and limited gel formation as indicated XRD and SEM-EDS data. The increase of Ms up to 1.0 and 2.0 results in a dense and compact microstructure, observed in SEM micrographs, as the sodium silicate provides additional silicon species that play a crucial role in the geopolymerization process. The slight decrease in mechanical properties when an excess of sodium silicate is used (Ms = 2.0) is due to the rapid precipitation of hydration products on the precursor grains, inhibiting their dissolution and alkaline activation reactions. As a result, there are smaller amounts of gel formed according to FTIR and SEM data, reducing the bonding between particles, and leaving some of them unreacted, leading to a consequent decline in mechanical properties.
4) XRD and FTIR analysis indicates the formation of N-A-S-H, C-(A)-S-H or N,C-A-S-H gels in all samples, as well as the presence of non-reactive crystalline phases. The activator modulus influences the degree of polymerization of the gels, obtaining more polymerized gels when using a Ms = 1.0.
5) SEM-EDS analysis confirms that the alkaline activation of the calcium-rich CDW precursor gives as main reaction product, C-A-S-H gel. The progressive addition of chamotte, which is richer in alumina and has lower calcium content, promotes the formation of geopolymeric gel or N-A-S-H gel, leading to the formation of the hybrid (C,N)-A-S-H gel responsible for the increase in mechanical properties. The use of Ms = 0.5 results in a porous structure, while the use of Ms = 2.0 results in a compact structure but with shrinkage cracks, both AACs having a high amount of unreacted particles.

The utilization of CDW residues rich in concrete fraction and the enrichment of the ceramic fraction through the incorporation of CHM as a raw material for the production of environmentally friendly alkali-activated cements, represents a highly effective pathway for the valorization of construction waste, aligning with the principles of circular economy. The incorporation of CHM and an appropriate activator module results in AACs with excellent mechanical performance. It is recommended to incorporate 40 wt% of CHM and use an activator module of Ms = 1.0.

## CRediT authorship contribution statement

**A. García-Díaz:** Writing – review & editing, Writing – original draft, Validation, Methodology, Investigation, Formal analysis, Data curation, Conceptualization. **P. Delgado-Plana:** Writing – review & editing, Methodology, Formal analysis, Data curation. **S. Bueno-Rodríguez:** Writing – review & editing, Validation, Methodology, Formal analysis, Conceptualization. **D. Eliche-Quesada:** Writing – review & editing, Writing – original draft, Resources, Project administration, Investigation, Formal analysis, Data curation,

Conceptualization.

## Declaration of competing interest

The authors declare that they have no known competing financial interests or personal relationships that could have appeared to influence the work reported in this paper.

## Data availability

Data will be made available on request.

## Acknowledgements

This work has been funded by the project GEOCIRCULA: Circular economy in the manufacture of new geopolymer composites: towards the goal of zero waste (P18-RT-3504). Regional Ministry of Economy, Knowledge, Business and University of the Junta de Andalucía. General Secretariat of Universities, Research and Technology/FEDER ″A way of doing Europe". The authors thank to the Association of Management Companies Construction and Demolition Waste (AGRECA)" and Ladrillos Bailén S.A. company for supplying the CDW and chamotte waste. Technical and human support provided by CICT of Universidad de Jaén (UJA, MINECO, Junta de Andalucía, FEDER) is gratefully acknowledged.

## References

[1] J.M. Moreno-Maroto, P. Delgado-Plana, R. Cabezas-Rodríguez, R. Mejía de Gutiérrez, D. Eliche-Quesada, Alkaline activation of high-crystalline low-$Al_2O_3$ Construction and Demolition Wastes to obtain geopolymers, J. Clean. Prod. 330 (2022) 129770, https://doi.org/10.1016/j.jclepro.2021.129770.
[2] R.A. Robayo-Salazar, W. Valencia-Saavedra, R. Mejía de Gutiérrez, Construction and demolition waste (CDW) recycling as both binder and aggregates in alkali-activated materials: a novel re-use concept, Sustainability 12 (2020) 1–18, https://doi.org/10.3390/su12145775.
[3] R. Islam, T. Hassan Nazifa, A. Yuniarto, A.S.M. Shanawaz Uddin, S. Salmiati, Sh Shahid, An empirical study of construction and demolition waste generation and implication of recycling, Waste Manag. 95 (2019) 10–21, https://doi.org/10.1016/j.wasman.2019.05.049.
[4] M. Bassani, L. Tefa, P. Palmero, The Alkali-Activation of Construction and Demolition Waste Components for Stabilization Purposes, International Conference on Sustainable Solid Waste Managemen, Naxos Island (Greece), 2018.
[5] R.A. Robayo-Salazar, J.F. Rivera, R. Mejía de Gutiérrez, Alkali-activated building materials made with recycled construction and demolition wastes, Construct. Build. Mater. 149 (2017) 130–138, https://doi.org/10.1016/j.conbuildmat.2017.05.122.
[6] M.V. Borrachero, J. Payá, S. Brito, Y.P. Segura, L. Soriano, M.M. Tashima, J.M. Monzó, Reusing construction and demolition waste to prepare alkali-activated cement, Materials 15 (2022) 3437, https://doi.org/10.3390/ma15103437.
[7] N. Cristelo, A. Fernández-Jiménez, C. Vieira, T. Miranda, A. Palomo, Stabilisation of construction and demolition waste with a high fines content using alkali activated fly ash, Construct. Build. Mater. 170 (2018) 26–39, https://doi.org/10.1016/j.conbuildmat.2018.03.057.
[8] M. Panizza, M. Natali, E. Garbin, S. Tamburini, M. Secco, Assessment of geopolymers with Construction and Demolition Waste (CDW) aggregates as a building material, Construct. Build. Mater. 181 (2018) 119–133, https://doi.org/10.1016/j.conbuildmat.2018.06.018.
[9] A. Allahverdi, E.N. Kani, Use of construction and demolition waste (CDW) for alkali-activated or geopolymer cements, Handbook of Recycled Concrete and Demolition Waste, Elsevier (2013) 439–475, https://doi.org/10.1533/9780857096906.3.439.
[10] M.A. Villaquirán-Caicedo, R. Mejía de Gutiérrez, Comparison of different activators for alkaline activation of construction and demolition wastes, Construct. Build. Mater. 281 (2021) 122599, https://doi.org/10.1016/j.conbuildmat.2021.122599.
[11] V. Bilsen, D. Kretz, P. Padilla, M. Van Acoleyen, J. Van Ostaeyen, O. Izdebska, M. Hansen, J. Bergmans, P. Szuppinger, Development and implementation of initiatives fostering investment and innovation in construction and demolition waste recycling infrastructure, European Commission (2018), https://doi.org/10.2873/11837.
[12] Z. Abdollahnejad, M. Mastali, M. Falah, T. Luukkonen, M. Mazari, M. Illikainen, Construction and demolition waste as recycled aggregates in alkali-activated concretes, Materials 12 (2019) 4016, https://doi.org/10.3390/ma12234016.
[13] J. Tan, J. Cai, J. Li, Recycling of unseparated construction and demolition waste (UCDW) through geopolymer technology, Construct. Build. Mater. 341 (2022) 127771, https://doi.org/10.1016/j.conbuildmat.2022.127771.
[14] S. Dadsetan, H. Siad, M. Lachemi, M. Sahmaran, Construction and demolition waste in geopolymer concrete technology: a review, Mag. Concr. Res. 71 (2019) 1232–1252, https://doi.org/10.1680/jmacr.18.00307.
[15] M. Bassani, L. Tefa, A. Russo, P. Palmero, Alkali-activation of recycled construction and demolition waste aggregate with no added binder, Construct. Build. Mater. 205 (2019) 398–413, https://doi.org/10.1016/j.conbuildmat.2019.02.031.
[16] A. Vásquez, V. Cárdenas, R.A. Robayo, R. Mejía de Gutiérrez, Geopolymer based on concrete demolition waste, Adv. Powder Technol. 27 (2016) 1173–1179, https://doi.org/10.1016/j.apt.2016.03.029.
[17] F.P. da Costa, I.M.T. Bezerra, J.V. Fernandes, A.M. Rodrigues, R.R. Menezes, G. de A. Neves, Durability of sustainable ceramics produced by alkaline activation of clay brick residue, Sustainability 13 (2021) 10931, https://doi.org/10.3390/su131910931.
[18] D. Zaharaki, M. Galetakis, K. Komnitsas, Valorization of construction and demolition (C&D) and industrial wastes through alkali activation, Construct. Build. Mater. 12 (2019) 686–693, https://doi.org/10.1016/j.conbuildmat.2016.06.051.
[19] A.R.G. Azevedo, C.M.F. Vieira, W.M. Ferreira, K.C.P. Faria, L.G. Pedroti, B.C. Mendes, Potential use of ceramic waste as precursor in the geopolymerization reaction for the production of ceramic roof tiles, J. Build. Eng. 29 (2020) 101156, https://doi.org/10.1016/j.jobe.2019.101156.
[20] S.A. Bernal, R. Mejía de Gutiérrez, J.L. Provis, V. Rose, Effect of silicate modulus and metakaolin incorporation on the carbonation of alkali silicate-activated slags, Cement Concr. Res. 40 (2010) 898–907, https://doi.org/10.1016/j.cemconres.2010.02.00.
[21] D. Eliche-Quesada, A. Calero-Rodríguez, E. Bonet-Martínez, L. Pérez-Villarejo, P.J. Sánchez-Soto, Geopolymers made from metakaolin sources, partially replaced by Spanish clays and biomass bottom ash, J. Build. Eng. 40 (2021) 102761, https://doi.org/10.1016/j.jobe.2021.102761.
[22] M.F. Zawrah, R.A. Gado, N. Feltin, S. Ducourtieux, L. Devoille, Recycling and utilization assessment of waste fired clay bricks (Grog) with granulated blast-furnace slag for geopolymer production, PSEP 103 (2016) 237–251, https://doi.org/10.1016/j.psep.2016.08.001.
[23] M. Ezzat, H.M. Khater, A.M. Elnagar, Enhanced characteristics of alkali activated slag/grog geopolymer bricks, Int. J. Sci. Eng. Res. 7 (2016) 230–243. ISSN 2229-5518.
[24] E. Sassoni, P. Pahlavan, E. Franzoni, M.C. Bignozzi, Valorization of brick waste by alkali-activation: a study on the possible use for masonry repointing, Ceram. Int. 42 (2016) 14685–14694, https://doi.org/10.1016/j.ceramint.2016.06.093.
[25] J.M. Terrones-Saeta, J. Suárez-Macías, F.J. Iglesias-Godino, F.A. Corpas-Iglesias, Development of geopolymers as substitutes for traditional ceramics for bricks with chamotte and biomass bottom ash, Materials 14 (2021) 1–20, https://doi.org/10.3390/ma14010199.

[26] G.F. Huseien, A.R.M. Sam, K.W. Shah, M.A. Asaad, M.M. Tahir, J. Mirza, Properties of ceramic tile waste-based alkali-activated mortars incorporating GBFS and fly ash, Construct. Build. Mater. (2019) 355–368, https://doi.org/10.1016/j.conbuildmat.2019.04.154.

[27] R.A. Gado, M. Hebda, M. Lach, J. Mikula, Alkali activation of waste clay bricks: influence of the silica modulus, $SiO_2/Na_2O$, $H_2O/Na_2O$ molar ratio, and liquid/solid ratio, Materials 13 (2020) 383, https://doi.org/10.3390/ma13020383.

[28] L. Reig, M.M. Tashima, M.V. Borrachero, J. Monzó, C.R. Cheeseman, J. Payá, Properties and microstructure of alkali-activated red clay brick waste, Construct. Build. Mater. 43 (2013) 98–106, https://doi.org/10.1016/j.conbuildmat.2013.01.031.

[29] M.C. Bignozzi, O. Fusco, A. Fregni, L. Guardigli, R. Gulli, Ceramic waste as new precursors for geopolymerization, Adv. Sci. Technol. 92 (2014) 26–31. https://doi.org/10.4028/www.scientific.net/AST.92.26.

[30] B.C. Mendes, L.C. Pedroti, C.M. Vieira, J.M. Carvalho, J.C. Ribeiro, N.M. Albuini-Oliveira, I.K. Andrade, Evaluation of eco-efficient geopolymer using chamotte and waste glass-based alkaline solutions, Case Stud. Constr. Mater. 16 (2022) e00847, https://doi.org/10.1016/j.cscm.2021.e00847.

[31] G.S. Ryu, Y.B. Lee, K.T. Koh, Y.S. Chung, The mechanical properties of fly ash-based geopolymer concrete with alkaline activators, Construct. Build. Mater. 47 (2013) 409–418, https://doi.org/10.1016/j.conbuildmat.2013.05.069.

[32] S. França, M.V. de Moura Solar Silva, P.H. Ribeiro Borges, A.C. da Silva Bezerra, A review on some properties of alkali-activated materials, Innov. Infrastruct. Solut. 7 (2022) 179, https://doi.org/10.1007/s41062-022-00789-w.

[33] M. Alhawat, A. Ashour, G. Yildirim, A. Aldemir, M. Sahmaran, Properties of geopolymers sourced from construction and demolition waste: a review, J. Build. Eng. 50 (2022) 104104, https://doi.org/10.1016/j.jobe.2022.104104.

[34] T. Phoo-Ngernkham, A. Maegawa, N. Mishima, S. Hatanaka, P. Chindaprasirt, Effects of sodium hydroxide and sodium silicate solutions on compressive and shear bond strengths of FA-GBFS geopolymer, Construct. Build. Mater. 91 (2015) 1–8, https://doi.org/10.1016/j.conbuildmat.2015.05.001.

[35] T. Phoo-ngernkham, S. Hanjitsuwan, N. Damrongwiriyanupap, P. Chindaprasirt, Effect of sodium hydroxide and sodium silicate solutions on strengths of alkali activated high calcium fly ash containing Portland cement, KSCE J. Civ. Eng. 21 (2017) 2202–2210, https://doi.org/10.1007/s12205-016-0327-6.

[36] A. Fernández-Jiménez, A. Palomo, Composition and microstructure of alkali activated fly ash binder: effect of the activator, Cement Concr. Res. 35 (2005) 1984–1992, https://doi.org/10.1016/j.cemconres.2005.03.003. Oct. 2005.

[37] C.R. Kaze, J.N. Yankwa-Djobo, A. Nana, H. Tchakoute, E. Kamseu, U.C. Melo, C. Leonelli, H. Rahier, Effect of silicate modulus on the setting, mechanical strength and microstructure of iron-rich aluminosilicate (laterite) based-geopolymer cured at room temperature, Ceram. Int. 44 (2018) 21442–21450, https://doi.org/10.1016/j.ceramint.2018.08.205.

[38] A. Allahverdi, E.N. Kani, S. Esmaeilpoor, Effects of silica modulus and alkali concentration on activation of blast-furnace slag, Iran, J. Mater. Sci. Eng. 5 (2008) 32–35.

[39] UNE-EN 1015-11:2000/A1, Methods of Test for Mortar for Masonry - Part 11: Determination of Flexural and Compressive Strength of Hardened Mortar, 2007.

[40] UNE-EN 1015-10, Methods of Test for Mortar for Masonry - Part 10: Determination of Dry Bulk Density of Hardened Mortar, 2000.

[41] ISO-8302, Thermal Insulation - Determination of Steady-State Thermal Resistance and Related Properties - Guarded Hot Plate Apparatus, 1991.

[42] M.A. Gómez-Casero, L. Pérez-Villarejo, E. Castro, D. Eliche-Quesada, Effect of steel slag and curing temperature on the improvement in technological properties of biomass bottom ash-based alkali-activated materials, Construct. Build. Mater. 302 (2021) 124205, https://doi.org/10.1016/j.conbuildmat.2021.124205.

[43] M.L. Gualtieri, A.F. Gualtieri, S. Gagliardi, P. Ruffini, R. Ferrari, M. Hanuskova, Thermal conductivity of fired clays: effects of mineralogical and physical properties of the raw materials, Appl. Clay Sci. 49 (2010) 269–275, https://doi.org/10.1016/j.clay.2010.06.002.

[44] M.M. Ahmed, K.A.M. El-Naggar, D. Tarek, A. Ragab, H. Sameh, A.M. Zeyad, B.A. Tayeh, I.M. Maafa, A. Yousef, Fabrication of thermal insulation geopolymer bricks using ferrosilicon slag and alumina waste, Case Stud. Constr. Mater. 15 (2021) e00737, https://doi.org/10.1016/j.cscm.2021.e00737.

[45] R. He, N. Dai, Z. Wang, Thermal and mechanical properties of geopolymers exposed to high temperature: a literature review, Adv. Civ. Eng. (2020) 1–14, https://doi.org/10.1155/2020/7532703.

[46] Y. Mortada, E. Masad, R.B. Kogbara, B. Mansoor, T. Seers, A. Hammoud, A. Karaki, Development of $Ca(OH)_2$-based geopolymer for additive manufacturing using construction wastes and nanomaterials, Case Stud. Constr. Mater. 19 (2023) e02258, https://doi.org/10.1016/j.cscm.2023.e02258.

[47] M.R. Wang, D.C. Jia, P.G. He, Y. Zhou, Microstructural and mechanical characterization of fly ash cenosphere/metakaolin-based geopolymeric composites, Ceram. Int. 37 (2011) 1661–1666, https://doi.org/10.1016/j.ceramint.2011.02.010.

[48] O. Mahmoodi, H. Siad, M. Lachemi, S. Dadsetan, M. Sahmaran, Development and characterization of binary recycled ceramic tile and brick wastes-based geopolymers at ambient and high temperatures, Construct. Build. Mater. 301 (2021) 124138, https://doi.org/10.1016/j.conbuildmat.2021.124138.

[49] C.K. Yip, G.C. Lukey, J.S.J. Van Deventer, The coexistence of geopolymeric gel and calcium silicate hydrate at the early stage of alkaline activation, Cement Concr. Res. 35 (2005) 1688–1697, https://doi.org/10.1016/j.cemconres.2004.10.042.

[50] S. Jurado-Contreras, E. Bonet-Martínez, P.J. Sánchez-Soto, O. Gencel, D. Eliche-Quesada, Synthesis and characterization of alkali-activated materials containing biomass fly ash and metakaolin: effect of the soluble salt content of the residue, Arch. Civ. Mech. Eng. 22 (2022) 1–21, https://doi.org/10.1007/s43452-022-00444-2.

[51] T. Ye, J. Xiao, Z. Duan, S. Li, Geopolymers made of recycled brick and concrete powder – a critical review, Construct. Build. Mater. 330 (2022) 127232, https://doi.org/10.1016/j.conbuildmat.2022.127232.

[52] H.-L. Chiang, C.P. Huang, P.C. Chiang, The surface characteristics of activated carbon as affected by ozone and alkaline treatmen, Chemosphere 47 (2022) 257–265, https://doi.org/10.1016/S0045-6535(01)00215-6.

[53] J.F. Rivera, N. Cristelo, A. Fernández-Jiménez, R. Mejía de Gutiérrez, Synthesis of alkaline cements based on fly ash and metallurgic slag: optimisation of the $SiO_2/Al_2O_3$ and $Na_2O/SiO_2$ molar ratios using the response surface methodology, Construct. Build. Mater. 213 (2019) 424–433, https://doi.org/10.1016/j.conbuildmat.2019.04.097.

[54] M.A. Gómez-Casero, C. De Dios-Arana, J.S. Bueno-Rodríguez, L. Pérez-Villarejo, D. Eliche-Quesada, Physical, mechanical and thermal properties of metakaolin-fly ash geopolymers, Sustain. Chem. Pharm. 26 (2022) 100620, https://doi.org/10.1016/j.scp.2022.100620.

[55] E. Bonet-Martínez, P. García-Cobo, L. Pérez-Villarejo, E. Castro, D. Eliche-Quesada, Effect of olive-pine bottom ash on properties of geopolymers based on metakaolin, Materials 13 (2020) 1–19, https://doi.org/10.3390/ma13040901.

[56] M. Liu, D. Yang, L. Chen, G. Chen, Z. Ma, Effect of silicate modulus and alkali content on the microstructure and macroscopic properties of alkali-activated recycled powder mortar, Construct. Build. Mater. 397 (2023) 132365, https://doi.org/10.1016/j.conbuildmat.2023.132365.

[57] A.V. Lăzărescu, H. Szilagyi, C. Baeră, A. Ioani, The effect of alkaline activator ratio on the compressive strength of fly ash-based geopolymer paste, IOP Conf: Mater. Sci. Eng. 209 (2017) 012064, https://doi.org/10.1088/1757-899X/209/1/012064.

[58] R.A. Robayo, A. Mulford, J. Munera, R. Mejía de Gutiérrez, Alternative cements based on alkali-activated red clay brick waste, Construct. Build. Mater. 128 (2016) 163–169, https://doi.org/10.1016/j.conbuildmat.2016.10.023.

[59] X. Ouyang, Y. Ma, Z. Liu, J. Liang, G. Ye, Effect of the sodium silicate modulus and slag content on fresh and hardened properties of alkali-activated fly ash/slag, Minerals 10 (2020) 1–17, https://doi.org/10.3390/min10010015.

[60] D. Eliche-Quesada, E. Bonet-Martínez, L. Pérez-Villarejo, E. Castro, P.J. Sánchez-Soto, Effects of an illite clay substitution on geopolymer synthesis as an alternative to metakaolin, J. Mater. Civ. Eng. 33 (2021) 1–19, https://doi.org/10.1061/(ASCE)MT.1943-5533.00036.

[61] X. Gao, Q.L. Yu, H.J.H. Brouwers, Reaction kinetics, gel character and strength of ambient temperature cured alkali activated slag-fly ash blends, Construct. Build. Mater. 80 (2015) 105–115, https://doi.org/10.1016/j.conbuildmat.2015.01.065.